INTERNATIONAL JOURNAL FOR NUMERICAL METHODS IN FLUIDS
Int. J. Numer. Meth. Fluids **30**: 1043–1066 (1999)

A DISTRIBUTED LAGRANGE MULTIPLIER/FICTITIOUS DOMAIN METHOD FOR FLOWS AROUND MOVING RIGID BODIES: APPLICATION TO PARTICULATE FLOW

ROLAND GLOWINSKI[a,b,*], TSORNG-WHAY PAN[b], TODD I. HESLA[c], DANIEL D. JOSEPH[c] AND JACQUES PÉRIAUX[d]

[a] *Université Pierre et Marie Curie, Paris, France*
[b] *Department of Mathematics, University of Houston, Houston, TX 77204, USA*
[c] *Department of Aerospace Engineering and Mechanics, University of Minnesota, Minneapolis, MN 55455, USA*
[d] *Dassault Aviation, 92214 Saint-Cloud, France*

SUMMARY

This article discusses the application of a Lagrange multiplier-based fictitious domain method to the numerical simulation of incompressible viscous flow modeled by the Navier–Stokes equations around moving rigid bodies; the rigid body motions are due to hydrodynamical forces and gravity. The solution method combines finite element approximations, time discretization by operator splitting and conjugate gradient algorithms for the solution of the linearly constrained quadratic minimization problems coming from the splitting method. The study concludes with the presentation of numerical results concerning four test problems, namely the simulation of an incompressible viscous flow around a NACA0012 airfoil with a fixed center but free to rotate, then the sedimentation of 200 and 1008 cylinders in a two-dimensional channel, and finally the sedimentation of two spherical balls in a rectangular cylinder.

KEY WORDS: particulate flow; fictitious domain method; Navier–Stokes equations

1. INTRODUCTION

Fictitious domain methods is a general term that covers in fact a large variety of solution methods for partial differential equations. Glowinski *et al.* [1–3] discussed fictitious domain methods based on *boundary supported Lagrange multipliers* to enforce *Dirichlet boundary conditions* and on regular structured meshes (which are not boundary fitted) over a simple shape auxiliary domain (the fictitious domain). These methods, initially developed for the solution of linear elliptic problems, have also been applied, as shown in the above references, to the solution of non-linear time-dependent problems, such as the variational inequalities modeling the flow of a viscous–plastic medium in a pipe, the Ginzburg–Landau equations, and the Navier–Stokes equations modeling incompressible viscous unsteady flow. For the simulation of flow around moving rigid bodies, where the motion is known, Glowinski *et al.* [4–6] have coupled a time discretization by operator splitting *à la* Marchuk–Yanenko with an L^2-projection technique that forces the incompressibility condition; the resulting method is robust, stable and easy to implement.

* Correspondence to: Department of Mathematics, University of Houston, Houston, TX 77204, USA.

CCC 0271–2091/99/161043–26$17.50

Received 2 March 1998
Revised 8 September 1998

In this study the numerical simulation of incompressible viscous flow around moving rigid bodies when the rigid body motions are caused by hydrodynamical forces and gravity are considered; several applications can be mentioned, for example, fluidized beds, sedimentation, and blood flow around artificial heart valves. The method of choice is a *distributed Lagrange multiplier/fictitious domain method* that consists of filling the moving bodies by the surrounding fluid and impose rigid body motions to the fluid occupying the regions originally occupied by the rigid bodies; then the rigid body motion constraint is relaxed by using distributed Lagrange multipliers and a flow problem over the entire region is obtained. This approach is quite different from the one in References [4–6], which is concerned with the case where the rigid body motion is known. The advantage of fictitious domain methods is that there is no need to generate a new mesh at each time step, immediately after finding the new position of the rigid bodies. This is a very important issue since for three-dimensional particulate flow, generating moving meshes for simulating fluid–rigid body interactions is a highly non-trivial problem; this problem has been successfully addressed in, for example, [7], using a sophisticated methodology. The fictitious domain method described in this article provides an alternative where flow computations are performed on a fixed grid, while rigid body motion is taken care of via a simple mesh that can be generated very quickly. Also (this is not specific to fictitious domain methods, see for example [8]), there is no need to compute the hydrodynamical forces explicitly, since the interaction between fluid and rigid bodies is implicitly contained in the variational formulation at the foundation of the present methodology. This approach has been applied to simulate the flow around an NACA0012 airfoil that has a fixed center, but that is free to rotate due to hydrodynamical forces, and the motion of sedimenting rigid bodies in two- and three-dimensional channels and to capture the hydrodynamic interactions with the rigid bodies.

It should be mentioned that non-Lagrange multiplier-based fictitious domain methods have been used by Peskin and his collaborators [9–11] to simulate incompressible viscous flow in regions with elastic moving boundaries, and by LeVeque [12,13] for elliptic problems with discontinuous coefficients and singular sources and Stokes flow with elastic boundaries or surface tension.

2. A MODEL PROBLEM AND ITS FICTITIOUS DOMAIN FORMULATION

Let $B(t) = \mathsf{U}_{i=1}^{I} B_i(t)$, where $B_i(t)$ is the ith moving rigid body in the fluid and $\Omega \subset \mathbb{R}^d$ ($d = 2, 3$; see Figure 1 for a particular case where $d = 2$). We consider for $t > 0$ the solution of the *Navier–Stokes equations*

$$\rho_{\mathrm{f}}\left(\frac{\partial \mathbf{u}}{\partial t} + (\mathbf{u}\cdot\nabla)\mathbf{u}\right) = \rho_{\mathrm{f}}\mathbf{g} + \nabla\cdot\sigma \quad \text{in } \Omega\backslash\overline{B(t)}, \tag{1}$$

$$\nabla\cdot\mathbf{u} = 0 \quad \text{in } \Omega\backslash\overline{B(t)}, \tag{2}$$

$$\mathbf{u}(\mathbf{x}, 0) = \mathbf{u}_0(\mathbf{x}), \quad \mathbf{x}\in\Omega\backslash\overline{B(0)} \ (\text{with } \nabla\cdot\mathbf{u}_0 = 0), \tag{3}$$

$$\mathbf{u} = \mathbf{g}_0 \quad \text{on } \Gamma, \tag{4}$$

to be completed by boundary conditions on $\partial B(t)$, given hereafter (see relation (8)). In (1)–(4) $\sigma = -p\mathbf{I} + \nu_{\mathrm{f}}(\nabla\mathbf{u} + (\nabla\mathbf{u})^T)$ is the stress sensor, $\mathbf{u}$ ($= \{u_i\}_{i=1}^{d}$) and p denote, as usual, velocity and pressure respectively; ρ_{f} is the density of the fluid, ν_{f} (> 0) is the fluid viscosity, $\mathbf{g}$ is the gravity, $\mathbf{x}$ the generic point of $\mathbb{R}^d$ ($\mathbf{x} = \{x_i\}_{i=1}^{d}$), $\overline{B(t)}$ the closure of the region occupied by $B(t)$, $\Gamma = \partial\Omega$, and

$$(\mathbf{u}\cdot\nabla)\mathbf{u} = \left\{\sum_{j=1}^{j=d} u_j \frac{\partial u_i}{\partial x_j}\right\}_{i=1}^{i=d}.$$

From the rigid body motion of the rigid bodies, $\mathbf{g}_0$ has to satisfy $\int_\Gamma \mathbf{g}_0\cdot\mathbf{n}\,\mathrm{d}\Gamma = 0$, where $\mathbf{n}$ is the outer normal unit vector at Γ (we suppose the no-slip condition on the boundary of each rigid body). In the following, we shall use, if necessary, the notation $\phi(t)$ for the function $\mathbf{x}\to\phi(\mathbf{x}, t)$.

For simplicity, we consider two-dimensional cases only (we can easily extend the following approach to three-dimensional cases). Assuming that the rigid bodies do not touch each other or the wall, we have from Newton's law, for the ith rigid body

$$M_{\mathrm{p},i}\frac{\mathrm{d}V_{\mathrm{p},i}}{\mathrm{d}t} = M_{\mathrm{p},i}\mathbf{g} + F_{\mathrm{p},i}, \tag{5}$$

$$I_{\mathrm{p},i}\frac{\mathrm{d}\omega_{\mathrm{p},i}}{\mathrm{d}t} = T_{\mathrm{p},i}, \tag{6}$$

$$\frac{\mathrm{d}G_{\mathrm{p},i}}{\mathrm{d}t} = V_{\mathrm{p},i}, \tag{7}$$

where $V_{\mathrm{p},i}$ is the translation velocity of the rigid body, $\omega_{\mathrm{p},i}$ is the angular velocity of the rigid body, $M_{\mathrm{p},i}$ is the mass of the rigid body, $I_{\mathrm{p},i}$ is the moment of inertia of the rigid body at $G_{\mathrm{p},i}$, $G_{\mathrm{p},i}$ being the center of mass of the rigid body; $\mathbf{g}$ is the gravity, $F_{\mathrm{p},i}$ is the force imposed on the rigid body by the fluid, $T_{\mathrm{p},i}$ is the moment imposed on the rigid body by the fluid. The boundary condition on the boundary $\Gamma_{\mathrm{p},i}(t)$ of the ith rigid body is

$$\mathbf{u} = V_{\mathrm{p},i} + \omega_{\mathrm{p},i}\times(\mathbf{x} - G_{\mathrm{p},i}), \quad \text{for } \mathbf{x}\in\Gamma_{\mathrm{p},i}(t). \tag{8}$$

The force and moment imposed on the rigid body by the fluid are described as follows:

$$F_{\mathrm{p},i} = \int_{\Gamma_{\mathrm{p},i}(t)} \sigma\mathbf{n}\,\mathrm{d}\gamma, \tag{9}$$

$$T_{\mathrm{p},i} = \int_{\Gamma_{\mathrm{p},i}(t)} (\mathbf{x} - G_{\mathrm{p},i})\times(\sigma\mathbf{n})\,\mathrm{d}\gamma, \tag{10}$$

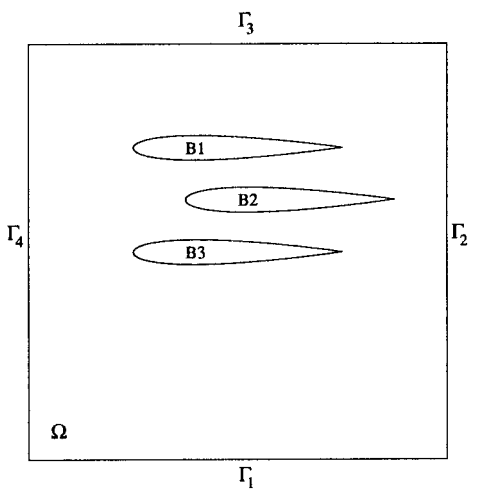

Figure 1. An example of two-dimensional flow region and rigid bodies.

where $\mathbf{x}$ is the generic point of $\mathbb{R}^2$ and $\mathbf{n}$ is the pointing outward unit normal vector on $\Gamma_{p,i}(t)$. In order to treat possible collisions either between rigid bodies or between rigid body and wall (or to avoid penetration either between rigid bodies or between rigid body and wall), which is a new problem posed by the direct simulation of fluidized suspensions, we shall substitute to the *momentum equation* in (5) the following one:

$$M_{p,i}\frac{dV_{p,i}}{dt} = M_{p,i}\mathbf{g} + F_{p,i} + F^r_{p,i}, \tag{11}$$

where $F^r_{p,i}$ is a lubrication force [14,15] imposed on the ith rigid body by the other rigid bodies and the walls.

For simplicity, we shall consider up to Section 5 the one rigid body case only. To obtain a variational formulation for problem (1)–(6), we define the following spaces:

$$\mathbf{V}_{\mathbf{g}_0(t)} = \{\mathbf{v}|\mathbf{v}\in H^1(\Omega\backslash\overline{B(t)})^2,\ \mathbf{v} = \mathbf{g}_0(t)\ \text{ on }\ \Gamma,\ \mathbf{v} = V_p(t) + \omega_p(t)\times(\mathbf{x} - G_p)\ \text{ on }\ \Gamma_p(t)\}, \tag{12}$$

$$\mathbf{V}_0 = \{\mathbf{v}|\mathbf{v}\in H^1(\overline{B(t)})^2,\ \mathbf{v} = 0\ \text{ on }\ \Gamma,\ \mathbf{v} = Y + \theta\times(\mathbf{x} - G_p)\ \text{ on }\ \Gamma_p(t),\ Y\in\mathbb{R}^2,\ \theta\in\mathbb{R}\}, \tag{13}$$

$$L^2_0(\Omega\backslash\overline{B(t)}) = \left\{q|q\in L^2(\Omega\backslash\overline{B(t)}),\ \int_{\Omega\backslash\overline{B(t)}} q\ d\mathbf{x} = 0\right\}. \tag{14}$$

It can be shown that the variational formulation of problem (1)–(6) is (if we include the collision forces)

For a.e. $t > 0$, find $\mathbf{u}(t)\in\mathbf{V}_{\mathbf{g}_0(t)}$, $p(t)\in L^2_0(\Omega\backslash\overline{B(t)})$, $(V_p(t), \omega_p(t))\in\mathbb{R}^3$, such that

$$\rho_f\int_{\Omega\backslash\overline{B(t)}}\frac{\partial\mathbf{u}}{\partial t}\cdot\mathbf{v}\,d\mathbf{x} + \rho_f\int_{\Omega\backslash\overline{B(t)}}(\mathbf{u}\cdot\nabla)\mathbf{u}\cdot\mathbf{v}\,d\mathbf{x} - \int_{\Omega\backslash\overline{B(t)}} p\nabla\cdot\mathbf{v}\,d\mathbf{x} + 2\nu_f\int_{\Omega\backslash\overline{B(t)}} D(\mathbf{u}) : D(\mathbf{v})\,d\mathbf{x}$$
$$+ Y\cdot\left(M_p\frac{dV_p}{dt} - M_p\mathbf{g}\right) + \theta I_p\frac{d\omega_p}{dt} - F^r_p\cdot Y = \int_{\Omega\backslash\overline{B(t)}}\rho_f\mathbf{g}\cdot\mathbf{v}\,d\mathbf{x},\quad \forall\mathbf{v}\in\mathbf{V}_0,\ Y\in\mathbb{R}^2,\ \theta\in\mathbb{R}, \tag{15}$$

$$\int_{\Omega\backslash\overline{B(t)}} q\nabla\cdot\mathbf{u}(t)\,dx = 0,\quad \forall q\in L^2(\Omega\backslash\overline{B(t)}), \tag{16}$$

$$\mathbf{u}(\mathbf{x}, 0) = \mathbf{u}_0(\mathbf{x}),\quad \mathbf{x}\in\Omega\backslash\overline{B(0)}\quad (\text{with }\ \nabla\cdot\mathbf{u}_0 = 0), \tag{17}$$

$$V_p(0) = V^0_p,\qquad \omega_p(0) = \omega^0_p, \tag{18}$$

where $D(\mathbf{v}) = (\nabla\mathbf{v} + (\nabla\mathbf{v})^T)/2$, $G_p(t) = G^0_p + \int_0^t V_p(s)\,ds$, V^0_p (respectively ω^0_p) are the initial velocity (respectively the initial angular velocity) of the rigid body $B(t)$ and G^0_p is the initial center position of the rigid body. To the best of our knowledge, this variational formulation, Equations (15)–(18), was introduced by Hesla [16]. Hu [8] also developed a similar variational formulation and combined it with an arbitrary Lagrange–Euler (ALE) technique. Hu has successfully simulated two-dimensional solid–liquid mixtures in a vertical channel with unstructured grids.

Now we fill the moving rigid body $B(t)$ by the surrounding fluid (imbed $\Omega\backslash\overline{B(t)}$ in Ω) and impose the rigid body motion to the fluid in the region originally occupied by the moving body. Then we relax the rigid body motion constraint by using distributed Lagrange multipliers and obtain a fictitious domain formulation over the entire region. Let us define the following spaces

$$\mathbf{W}_{\mathbf{g}_0(t)} = \{\mathbf{v}|\mathrm{v}\in H^1(\Omega)^2,\ \mathbf{v} = \mathbf{g}_0(t)\ \text{ on }\ \Gamma\},\qquad \mathbf{W}_0 = H^1_0(\Omega)^2, \tag{19}$$

$$L_0^2(\Omega) = \left\{ q \,|\, q \in L^2(\Omega),\ \int_\Omega q \ \mathrm{d}\mathbf{x} = 0 \right\}, \tag{20}$$

$$\Lambda(t) = H^1(B(t))^2. \tag{21}$$

To enforce the rigid body motion we can use, for example, the scalar product $\langle \cdot, \cdot \rangle_{B(t)}$ defined as follows:

$$\langle \mu, \mathbf{v} \rangle_{B(t)} = \int_{B(t)} (\mu \cdot \mathbf{v} + \nabla\mu : \nabla\mathbf{v}) \ \mathrm{d}\mathbf{x}, \quad \forall \mu \in H^1(B(t))^2, \quad \forall \mathbf{v} \in H^1(\Omega)^2. \tag{22}$$

The corresponding fictitious domain formulation of problem (15)–(18) is then

For a.e. $t > 0$, find $\mathbf{U}(t) \in \mathbf{W}_{\mathbf{g}_0(t)}$, $P(t) \in L_0^2(\Omega)$, $\lambda(t) \in \Lambda(t)$, $(V_\mathrm{p}(t), \omega_\mathrm{p}(t)) \in \mathbb{R}^3$, such that

$$\rho_\mathrm{f} \int_\Omega \frac{\partial \mathbf{U}}{\partial t} \cdot \mathbf{v} \ \mathrm{d}\mathbf{x} + \rho_\mathrm{f} \int_\Omega (\mathbf{U} \cdot \nabla)\mathbf{U} \cdot \mathbf{v} \ \mathrm{d}\mathbf{x} - \int_\Omega P \nabla \cdot \mathbf{v} \ \mathrm{d}\mathbf{x} + 2\nu_\mathrm{f} \int_\Omega D(\mathbf{U}) : D(\mathbf{v}) \ \mathrm{d}\mathbf{x}$$
$$+ \left(1 - \frac{\rho_\mathrm{f}}{\rho_\mathrm{s}}\right) M_\mathrm{p} \frac{\mathrm{d}V_\mathrm{p}}{\mathrm{d}t} \cdot Y + \left(1 - \frac{\rho_\mathrm{f}}{\rho_\mathrm{s}}\right) I_\mathrm{p} \frac{\mathrm{d}\omega_\mathrm{p}}{\mathrm{d}t} \theta - \left(1 - \frac{\rho_\mathrm{f}}{\rho_\mathrm{s}}\right) M_\mathrm{p} \mathbf{g} \cdot Y - F_\mathrm{p}^r \cdot Y$$
$$- \langle \lambda, \mathbf{v} - Y - \theta \times (\mathbf{x} - G_\mathrm{p}) \rangle_{B(t)} = \int_\Omega \rho_\mathrm{f} \mathbf{g} \cdot \mathbf{v} \ \mathrm{d}\mathbf{x}, \quad \forall \mathbf{v} \in \mathbf{W}_0, \ Y \in \mathbb{R}^2, \ \theta \in \mathbb{R}, \tag{23}$$

$$\int_\Omega q \nabla \cdot \mathbf{U}(t) \ \mathrm{d}\mathbf{x} = 0, \quad \forall q \in L^2(\Omega), \tag{24}$$

$$\langle \mu, \mathbf{U}(t) - V_\mathrm{p}(t) - \omega_\mathrm{p}(t) \times (\mathbf{x} - G_\mathrm{p}(t)) \rangle_{B(t)} = 0, \quad \forall \mu \in \Lambda(t), \tag{25}$$

$$\mathbf{U}(\mathbf{x}, 0) = \mathbf{U}_0(\mathbf{x}), \quad \mathbf{x} \in \Omega \quad (\text{with } \nabla \cdot \mathbf{U}_0 = 0), \tag{26}$$

$$V_\mathrm{p}(0) = V_\mathrm{p}^0, \qquad \omega_\mathrm{p}(0) = \omega_\mathrm{p}^0, \tag{27}$$

where $\mathbf{U}_0$ is an extension of $\mathbf{u}_0$ such that $\nabla \cdot \mathbf{U}_0 = 0$. Here we have $\mathbf{U}|_{\Omega \setminus \overline{B(t)}} = \mathbf{u}$ and $\mathbf{P}|_{\Omega \setminus \overline{B(t)}} = p$. The above formulation is due to the first two authors. In Equation (23), we can include the gravity term on the right-hand-side into the pressure term on the left-hand-side, as shall be done in the following sections.

Remark 2.1

Since in Equation (23) $\mathbf{U}$ is (obviously) divergence-free and satisfies the Dirichlet boundary conditions on Γ, we have

$$2 \int_\Omega D(\mathbf{U}) : D(\mathbf{v}) \ \mathrm{d}\mathbf{x} = \int_\Omega \nabla\mathbf{U} : \nabla\mathbf{v} \ \mathrm{d}\mathbf{x}, \quad \forall \mathbf{v} \in \mathbf{W}_0.$$

A substantial simplification, indeed, from a *computational point of view*, which is another plus for the fictitious domain approach used here. This simplification has been taken into account in the remaining parts of this article.

Remark 2.2

For *dimensionality* reasons, a H^1-scalar product more physical than the one defined by (22) is given by

$$\langle \mu, \mathbf{v} \rangle_{B(t)} = \int_{B(t)} (\mu \cdot \mathbf{v} + \alpha \nabla\mu : \nabla\mathbf{v}) \ \mathrm{d}x,$$

where α is a *scaling factor*; an obvious choice for α is to take it equal to d^2, where d is the *diameter* of the rigid body, which is clearly the most important characteristic length in the problem. Another natural H^1-scalar product, well-suited to rigid body motions, is

$$\langle \mu, \mathbf{v} \rangle_{B(t)} = \int_{B(t)} (\mu \cdot \mathbf{v} + 2\alpha D(\mu) : D(\mathbf{v}))\, \mathrm{d}\mathbf{x}.$$

3. FINITE ELEMENT APPROXIMATIONS

We still assume that $\Omega \subset \mathbb{R}^2$. With h a *space discretization* step we introduce a finite element triangulation $\mathscr{T}_h$ of $\bar{\Omega}$ and then $\mathscr{T}_{2h}$ a triangulation twice coarser (in practice we should construct $\mathscr{T}_{2h}$ first and then $\mathscr{T}_h$ by joining the midpoints of the edges of $\mathscr{T}_{2h}$, then dividing each triangle of $\mathscr{T}_{2h}$ into four similar subtriangles). We define the following finite-dimensional spaces that approximate $\mathbf{W}_{\mathbf{g}_0(t)}$, $\mathbf{W}_0$, $L^2(\Omega)$, $L^2_0(\Omega)$ respectively

$$\mathbf{W}_{\mathbf{g}_{0h}} = \{\mathbf{v}_h | \mathbf{v}_h \in C^0(\bar{\Omega})^2,\ \mathbf{v}_h|_T \in P_1 \times P_1,\ \forall T \in \mathscr{T}_h,\ \mathbf{v}_h|_\Gamma = \mathbf{g}_{0h}\}, \tag{28}$$

$$\mathbf{W}_{0h} = \{\mathbf{v}_h | \mathbf{v}_h \in C^0(\bar{\Omega})^2,\ \mathbf{v}_h|_T \in P_1 \times P_1,\ \forall T \in \mathscr{T}_h,\ \mathbf{v}_h|_\Gamma = 0\}, \tag{29}$$

$$L^2_h = \{q_h | q_h \in C^0(\bar{\Omega}),\ q_h|_T \in P_1,\ \forall T \in \mathscr{T}_{2h}\}, \qquad L^2_{0h} = \left\{ q_h | q_h \in L^2_h,\ \int_\Omega q_h\, \mathrm{d}\mathbf{x} = 0 \right\} \tag{30}$$

in (28)–(30), $\mathbf{g}_{0h}$ is an approximation of $\mathbf{g}_0$ satisfying $\int_\Gamma \mathbf{g}_{0h} \cdot \mathbf{n}\, \mathrm{d}\Gamma = 0$ and P_1 is the space of the polynomials in two variables of degree ≤ 1.

Let $\overline{B_h(t)}$ be a polygonal domain inscribed in $\overline{B(t)}$ and $\mathscr{T}_{B_h(t)}$ be a finite element triangulation of $B_h(t)$. Then a finite-dimensional space approximating $\Lambda(t)$ is

$$\Lambda_h(t) = \{\mu_h | \mu_h \in C^0(\overline{B_h(t)})^2,\ \mu_h|_T \in P_1 \times P_1,\ \forall T \in \mathscr{T}_{B_h(t)}\}. \tag{31}$$

An alternative to $\Lambda_h(t)$ defined by (31) is as follows: let $\{\mathbf{x}_i\}_{i=1}^{nd}$ be a set of points from $\overline{B(t)}$ that covers $\overline{B(t)}$ uniformly; we define then

$$\Lambda_h(t) = \left\{ \mu_h \middle| \mu_h = \sum_{i=1}^{nd} \mu_i \delta(\mathbf{x} - \mathbf{x}_i),\ \mu_i \in \mathbb{R}^2 \text{ for } i = 1, \ldots, nd \right\}, \tag{32}$$

where $\delta(\cdot)$ is the Dirac measure at $\mathbf{x} = 0$. Then, instead of the scalar product of $(H^1(B_h(t)))^2$ we shall use $\langle \cdot, \cdot \rangle_{B_h(t)}$ defined by

$$\langle \mu_h, \mathbf{v}_h \rangle_{B_h(t)} = \sum_{i=1}^{nd} \mu_i \cdot \mathrm{v}_h(\mathbf{x}_i), \quad \forall \mu_h \in \Lambda_h(t), \quad \mathbf{v}_h \in \mathbf{W}_{\mathbf{g}_{0h}} \text{ or } \mathbf{W}_{0h}. \tag{33}$$

Using the 'scalar product' defined by (33) implies that the rigid body motion of $B(t)$ is forced via a *collocation method*. A similar technique has been used to enforce the Dirichlet boundary conditions by Bertrand *et al.* [17] (other approaches are possible and will be investigated in the future).

Using those finite-dimensional spaces leads to the following approximation of problem (23)–(27):

$$\begin{aligned} &\rho_\mathrm{f} \int_\Omega \frac{\partial \mathbf{U}_h}{\partial t} \cdot \mathbf{v}\, \mathrm{d}\mathbf{x} + \rho_\mathrm{f} \int_\Omega (\mathbf{U}_h \cdot \nabla)\mathbf{U}_h \cdot \mathbf{v}\, \mathrm{d}\mathbf{x} - \int_\Omega P_h \nabla \cdot \mathbf{v}\, \mathrm{d}\mathbf{x} + \nu_\mathrm{f} \int_\Omega \nabla \mathbf{U}_h : \nabla \mathbf{v}\, \mathrm{d}\mathbf{x} \\ &+ \left(1 - \frac{\rho_\mathrm{f}}{\rho_\mathrm{s}}\right) M_\mathrm{p} \frac{\mathrm{d}V_\mathrm{p}}{\mathrm{d}t} \cdot Y + \left(1 - \frac{\rho_\mathrm{f}}{\rho_\mathrm{s}}\right) I_\mathrm{p} \frac{\mathrm{d}\omega_\mathrm{p}}{\mathrm{d}t}\, \theta - \left(1 - \frac{\rho_\mathrm{f}}{\rho_\mathrm{s}}\right) M_\mathrm{p} \mathbf{g} \cdot Y - F^r_\mathrm{p} \cdot Y \\ &- \langle \lambda_h, \mathbf{v} - Y - \theta \times (\mathbf{x} - G_\mathrm{p}) \rangle_{B_h(t)} = 0, \quad \forall \mathbf{v} \in \mathbf{W}_{0h}, \quad Y \in \mathbb{R}^2, \quad \theta \in \mathbb{R}, \end{aligned} \tag{34}$$

$$\int_\Omega q \nabla \cdot \mathbf{U}_h(t)\, \mathrm{dx} = 0, \quad \forall q \in L^2_h, \tag{35}$$

$$\langle \mu, \mathbf{U}_h(t) - V_p(t) - \omega_p(t) \times (\mathbf{x} - G_p(t)) \rangle_{B_h(t)} = 0, \quad \forall \mu \in \Lambda_h(t), \tag{36}$$

$$\mathbf{U}_h(0) = \mathbf{U}_{0h}, \quad \mathbf{x} \in \Omega, \quad V_p(0) = V_p^0, \quad \omega_p(0) = \omega_p^0, \tag{37}$$

$$\{\mathbf{U}_h(t), P_h(t), \lambda_h(t), V_p, \omega_p\} \in \mathbf{W}_{\mathbf{g}_0(t)h} \times L^2_{0h} \times \Lambda_h(t) \times \mathbb{R}^3; \tag{38}$$

in (37), $\mathbf{U}_{0h}$ is an approximation of $\mathbf{U}_0$ so that $\int_\Omega q \nabla \cdot \mathbf{U}_{0h} \, d\mathbf{x} = 0$ for all $q \in L^2_h$.

Remark 3.1
We replaced, in relation (34), $2\int_\Omega D(\mathbf{U}) : D(\mathbf{v}) \, d\mathbf{x}$ by $\int_\Omega \nabla \mathbf{U} : \nabla \mathbf{v} \, d\mathbf{x}$ by taking remark 2.1 into account.

Remark 3.2
Formulation (34)–(38) involves two Lagrange multipliers, namely P_h, associated with the discrete incompressible constraint (35), and λ_h, associated with the discrete rigid body motion condition (36). Variational formulations such as (34)–(38) (and (23)–(27)) are known as mixed variational formulations. The approximation of mixed variational problems is discussed in detail in Brezzi and Fortin [18] and Roberts and Thomas [19]. In order to explain the issues at stake to the unfamiliar reader, consider the following simple mixed variational problem

$$\begin{cases} a(u, v) + b(\lambda, v) = L(v), \quad \forall v \in V, \\ b(\mu, u) = 0, \quad \forall \mu \in \Lambda, \\ \{u, \lambda\} \in V \times \Lambda, \end{cases} \tag{MVP}$$

where in (MVP):

- V and Λ are two real Hilbert spaces;
- $a: V \to \mathbb{R}$ is bilinear and continuous;
- $b: \Lambda \times V \to \mathbb{R}$ is bilinear and continuous;
- $L: V \to \mathbb{R}$ is linear and continuous.

Suppose that (MVP) has a unique solution (sufficient conditions for that are given in References [18,19]). In order to approximate (MVP) we introduce families $\{V_h\}_h$ and $\{\Lambda_h\}_h$ of subspaces of V and Λ respectively; h being a parameter so that $h \to 0$. We suppose that the following convergence property holds

$$\forall \{v, \mu\} \in V \times \Lambda, \text{ there exists a family } \{\{v_h, \mu_h\}\}_h \text{ so that } \{v_h, \mu_h\} \in V_h \times \Lambda_h, \ \forall h$$
$$\text{and } \lim_{h \to 0} (\|v - v_h\|_V + \|\mu - \mu_h\|_\Lambda) = 0. \tag{CP}$$

It make sense then to approximate (MVP) by

$$\begin{cases} a(u_h, v_h) + b(\lambda_h, v_h) = L(v_h), \quad \forall v_h \in V_h, \\ b(\mu_h, u_h) = 0, \quad \forall \mu_h \in \Lambda_h, \\ \{u_h, \lambda_h\} \in V_h \times \Lambda_h. \end{cases} \tag{MVP}_h$$

Suppose that problem $(\text{MVP})_h$ has a unique solution for all h. It is well known that in general we do not have

$$\lim_{h \to 0} \{u_h, \lambda_h\} = \{u, \lambda\}$$

unless there exist compatibility conditions between $\{V_h\}_h$ and $\{\Lambda_h\}_h$ implying the stability and convergence of the family $\{\{u_h, \lambda_h\}\}_h$ of approximate solutions (such conditions are discussed

in [18,19] for important classes of mixed variational problems originating from continuum mechanics). Similar conditions hold for problems (23)–(27) and (34)–(38). It has been shown, in particular by Girault and Glowinski (work in progress), that a Ladyzhenskaya–Babuska–Brezzi (LBB) condition implying stability and convergence is satisfied if the velocity and pressure spaces are defined by (28)–(30) and if (in the case of flow regions with fixed boundary) $h_B \simeq 2h_\Omega$, where, as easily guessed, h_B is the size of the mesh used to approximate Λ, and h_Ω is the size of the velocity grid. Actually, the above condition can be relaxed and we still observe stability and convergence if one takes $h_B \simeq \kappa h_\Omega$, with $1 < \kappa \leq 2$. Other approaches are possible in obtaining stability and convergence, like for example, those approaches based on regularization, described in [18] (see also the references therein).

4. TIME DISCRETIZATION BY OPERATOR SPLITTING

Following Chorin [20–22], most 'modern' Navier–Stokes solvers are based on operator splitting algorithms [23,24] in order to force the incompressibility condition via a Stokes solver or a L^2-projection method (see also Gresho and Sani [25] for detailed information on L^2-projection methods). This approach still applies to the initial value problem (34)–(38), which contains three numerical difficulties to each of which can be associated a specific operator, namely

(a) The incompressibility condition and the related unknown pressure.
(b) An advection–diffusion term.
(c) The rigid body motion of $B_h(t)$ and the related multiplier $\lambda_h(t)$.

The operators in (a) and (c) are essentially *projection operators*. From an abstract point of view, problem (34)–(38) is a particular case of the following class of initial value problems:

$$\frac{\mathrm{d}\phi}{\mathrm{d}t} + A_1(\phi) + A_2 + A_3(\phi) = f, \qquad \phi(0) = \phi_0, \tag{39}$$

where the operators A_i can be multivalued. Among the many operator splitting methods that can be employed to solve (39), we advocate the very simple one [26] below; it is only first-order-accurate but its low-order accuracy is compensated by good stability and robustness properties.

4.1. A fractional step scheme à la Marchuk–Yanenko

With Δt a time discretization step and the initial guess $\phi^0 = \phi_0$, this scheme is defined as follows:

for $n \geq 0$, we obtain ϕ^{n+1} from ϕ^n via the solution of

$$(\phi^{n+j/3} - \phi^{n+(j-1)/3})/\Delta t + A_j(\phi^{n+j/3}) = f_j^{n+1}, \tag{40}$$

with $j = 1, 2, 3$ and $\Sigma_{j=1}^{3} f_j^{n+1} = f^{n+1}$. Applying scheme (40) to problem (34)–(38) we obtain (with $0 \leq \alpha,\ \beta \leq 1,\ \alpha + \beta = 1$ and after dropping some of the subscripts h)

$$\mathbf{U}^0 = \mathbf{U}_{0h};\ V_{\mathrm{p}}^0,\ \omega_{\mathrm{p}}^0 \text{ and } G_{\mathrm{p}}^0 \text{ are given;} \tag{41}$$

for $n \geq 0$, knowing $\mathbf{U}^n$, V_{p}^n, ω_{p}^n, G_{p}^n, we compute $\mathbf{U}^{n+1/3}$, $\mathbf{P}^{n+1/3}$ via the solution of

$$\begin{cases} \rho_{\mathrm{f}} \displaystyle\int_{\Omega} \frac{\mathbf{U}^{n+1/3}-\mathbf{U}^{n}}{\Delta t}\cdot\mathbf{v}\,\mathrm{d}\mathbf{x} - \int_{\Omega} P^{n+1/3}\nabla\cdot\mathbf{v}\,\mathrm{d}\mathbf{x} = 0, \quad \forall \mathbf{v}\in\mathbf{W}_{0h}, \\ \displaystyle\int_{\Omega} q\nabla\cdot\mathbf{U}^{n+1/3}\,\mathrm{d}\mathbf{x} = 0, \quad \forall q\in L_h^2;\ \mathbf{U}^{n+1/3}\in\mathbf{W}_{\mathbf{g}_{0h}}^{n+1},\ P^{n+1/3}\in L_{0h}^2. \end{cases} \tag{42}$$

Then we compute $\mathbf{U}^{n+2/3}$ via the solution of

$$\rho_{\mathrm{f}}\int_{\Omega}\frac{\mathbf{U}^{n+2/3}-\mathbf{U}^{n+1/3}}{\Delta t}\cdot\mathbf{v}\,\mathrm{d}\mathbf{x} + \alpha\nu_{\mathrm{f}}\int_{\Omega}\nabla\mathbf{U}^{n+2/3}:\nabla\mathbf{v}\,\mathrm{d}\mathbf{x} + \rho_{\mathrm{f}}\int_{\Omega}(\mathbf{U}^{n+1/3}\cdot\nabla)\mathbf{U}^{n+2/3}\cdot\mathbf{v}\,\mathrm{d}\mathbf{x} = 0,$$
$$\forall\mathbf{v}\in\mathbf{W}_{0h};\ \mathbf{U}^{n+2/3}\in\mathbf{W}_{\mathbf{g}_{0h}}^{n+1}, \tag{43}$$

and then compute $V_{\mathrm{p}}^{n+2/3}$ and $G_{\mathrm{p}}^{n+2/3}$ via:

Take $V_{\mathrm{p}}^{n,0}=V_{\mathrm{p}}^{n}$, $G_{\mathrm{p}}^{n,0}=G_{\mathrm{p}}^{n}$; then predict the new position and translation velocity of the rigid body via the following subcycling technique

do $k=1, N$

$$V_{\mathrm{p}}^{*n,k} = V_{p}^{n,k-1} + \left(\mathbf{g}+\left(1-\frac{\rho_{\mathrm{f}}}{\rho_{\mathrm{s}}}\right)^{-1} M_{\mathrm{p}}^{-1}F^{r}(G_{\mathrm{p}}^{n,k-1})\right)\frac{\Delta t}{N}, \tag{44}$$

$$G_{\mathrm{p}}^{*n,k} = G_{\mathrm{p}}^{n,k-1} + (V_{\mathrm{p}}^{*n,k}+V_{\mathrm{p}}^{n,k-1})\frac{\Delta t}{2N}, \tag{45}$$

$$V_{\mathrm{p}}^{n,k} = V_{\mathrm{p}}^{n,k-1} + \mathbf{g}\frac{\Delta t}{N} + \left(1-\frac{\rho_{\mathrm{f}}}{\rho_{\mathrm{s}}}\right)^{-1} M_{\mathrm{p}}^{-1}(F^{r}(G_{\mathrm{p}}^{*n,k})+F^{r}(G_{\mathrm{p}}^{n,k-1}))\frac{\Delta t}{2N}, \tag{46}$$

$$G_{\mathrm{p}}^{n,k} = G_{\mathrm{p}}^{n,k-1} + (V_{\mathrm{p}}^{n,k}+V_{\mathrm{p}}^{n,k-1})\frac{\Delta t}{2N}, \tag{47}$$

enddo.

Set $V_{\mathrm{p}}^{n+2/3}=V_{\mathrm{p}}^{n,N}$, $G_{\mathrm{p}}^{n+2/3}=G_{\mathrm{p}}^{n,N}$.
Finally we compute $\mathbf{U}^{n+1}$, λ^{n+1}, V_{p}^{n+1}, $\omega_{\mathrm{p}}^{n+1}$ via the solution of

$$\begin{cases} \rho_{\mathrm{f}}\displaystyle\int_{\Omega}\frac{\mathbf{U}^{n+1}-\mathbf{U}^{n+2/3}}{\Delta t}\cdot\mathbf{v}\,\mathrm{d}\mathbf{x} + \beta\nu_{\mathrm{f}}\int_{\Omega}\nabla\mathbf{U}^{n+1}:\nabla\mathbf{v}\,\mathrm{d}\mathbf{x} + \left(1-\frac{\rho_{\mathrm{f}}}{\rho_{\mathrm{s}}}\right)I_{\mathrm{p}}\frac{\omega_{\mathrm{p}}^{n+1}-\omega_{\mathrm{p}}^{n}}{\Delta t}\theta \\ \quad + \left(1-\dfrac{\rho_{\mathrm{f}}}{\rho_{\mathrm{s}}}\right)M_{\mathrm{p}}\frac{V_{\mathrm{p}}^{n+1}-V_{\mathrm{p}}^{n+2/3}}{\Delta t}\cdot Y \\ \quad = \left\langle\lambda^{n+1}, \mathbf{v}-Y-\theta\times(\mathbf{x}-G_{\mathbf{p}}^{n+2/3})\right\rangle_{B_h^{n+2/3}}, \quad \forall\mathbf{v}\in\mathbf{W}_{0h},\ Y\in\mathbb{R}^2,\ \theta\in\mathbb{R}, \\ \left\langle\mu, \mathbf{U}^{n+1}-V_{\mathrm{p}}^{n+1}-\omega_{\mathrm{p}}^{n+1}\times(\mathbf{x}-G_{\mathrm{p}}^{n+2/3})\right\rangle_{B_h^{n+2/3}} = 0, \quad \forall\mu\in\Lambda_h^{n+2/3}; \\ \mathbf{U}^{n+1}\in\mathbf{W}_{\mathbf{g}_{0h}}^{n+1},\ \lambda^{n+1}\in\Lambda_h^{n+2/3},\ V_{\mathrm{p}}^{n+1}\in\mathbb{R}^2,\ \omega_{\mathrm{p}}^{n+1}\in\mathbb{R}; \end{cases} \tag{48}$$

then take $G_{\mathrm{p}}^{n+1,0}=G_{\mathrm{p}}^{n+2/3}$ and correct the position of the rigid body center as follows:

do $k=1, N$

$$G_{\mathrm{p}}^{*n+1,k} = G_{\mathrm{p}}^{n+1,k-1} + (V_{\mathrm{p}}^{n}+V_{\mathrm{p}}^{n+1})\frac{\Delta t}{2N}, \tag{49}$$

$$G_{\mathrm{p}}^{n+1,k} = G_{\mathrm{p}}^{*n+1,k} + \left(1 - \frac{\rho_{\mathrm{f}}}{\rho_{\mathrm{s}}}\right)^{-1} M_{\mathrm{p}}^{-1}(F^r(G_{\mathrm{p}}^{n+1,k-1}) + F^r(G_{\mathrm{p}}^{*n+1,k}))\,\frac{(\Delta t)^2}{4N^2}, \tag{50}$$

enddo.

Set $G_{\mathrm{p}}^{n+1} = G_{\mathrm{p}}^{n+1,N}$.

In (41)–(50) we have $\mathbf{W}_{\mathbf{g}_{0h}}^{n+1} = \mathbf{W}_{\mathbf{g}_0((n+1)\Delta t)h}$, $\Lambda_h^{n+s} = \Lambda_h((n+s)\Delta t)$ and $B_h^{n+s} = B_h((n+s)\Delta t)$. In (44)–(47) we predict the position of the rigid body center and use it in (48), then in (49) and (50) we correct the prediction of the rigid body center position. With operator splitting, we can use a smaller time step to predict and correct the position of the center of the rigid bodies without changing the time step of algorithm (41)–(50). For our numerical simulations, we have used $\alpha = 1$ and $\beta = 0$ in (41)–(50) and $N = 10$ in (44)–(47) and (49) and (50).

5. SOLUTION OF THE SUBPROBLEMS (42), (43) AND (48)

By inspection of (42) it is clear that $\mathbf{U}^{n+1/3}$ is the $L^2(\Omega)^2$-projection of $\mathbf{U}^n$ on the (affine) subset of the functions $\mathbf{v} \in \mathbf{W}_{\mathbf{g}_{0h}}^{n+1}$ such that $\int_\Omega q \nabla \cdot \mathbf{v}\, \mathrm{dx} = 0$, $\forall q \in L_h^2$, where $P^{n+1/3}$ is the corresponding Lagrange multiplier in L_{0h}^2. The pair $\{\mathbf{U}^{n+1/3}, P^{n+1/3}\}$ is *unique* and to compute it we can use an Uzawa/conjugate gradient algorithm operating in L_{0h}^2 equipped with the scalar product $\{q, q'\} \to \int_\Omega \nabla q \cdot \nabla q'\, \mathrm{d}\mathbf{x}$. We obtain an algorithm [6] preconditioned by the discrete equivalent of $-\Delta$ for the homogeneous Neumann boundary condition. Such an algorithm is very easy to implement and seems to have excellent convergence properties.

If $\alpha > 0$, problem (43) is a classical one; it can be easily solved, for example, by a least-squares/conjugate gradient algorithm [27].

The solution of problem (48) can be computed by algorithms similar to those described in [1] for elliptic problems, with the additional difficulty that there are three more equations here, namely the ones used to compute the translation velocity and angular speed of the rigid body. Problem (48) has the following form:

$$\begin{cases} \alpha \displaystyle\int_\Omega \mathbf{u}\cdot\mathbf{v}\, \mathrm{dx} + \nu \int_\Omega \nabla\mathbf{u} : \nabla\mathbf{v}\, \mathrm{dx} + \left(1 - \frac{\rho_{\mathrm{f}}}{\rho_{\mathrm{s}}}\right) I_{\mathrm{p}} \frac{\omega_{\mathrm{p}} - \omega_{\mathrm{p}0}}{\Delta t}\,\theta + \left(1 - \frac{\rho_{\mathrm{f}}}{\rho_{\mathrm{s}}}\right) M_{\mathrm{p}} \frac{V_{\mathrm{p}} - V_{\mathrm{p}0}}{\Delta t} \cdot Y \\ = \displaystyle\int_\Omega \mathbf{f}\cdot\mathbf{v}\, \mathrm{dx} + \langle \lambda, \mathbf{v} - Y - \theta \times (\mathbf{x} - G_{\mathrm{p}}) \rangle_{B_h}, \quad \forall \mathbf{v} \in \mathbf{W}_{0h},\ Y \in \mathbb{R}^2,\ \theta \in \mathbb{R}, \\ \langle \mu, \mathbf{u} - V_{\mathrm{p}} - \omega_{\mathrm{p}} \times (\mathbf{x} - G_{\mathrm{p}}) \rangle_{B_h} = 0, \quad \forall \mu \in \Lambda_h;\ \mathbf{u} \in \mathbf{W}_{\mathbf{g}_{0h}},\ \lambda \in \Lambda_h,\ V_{\mathrm{p}} \in \mathbb{R}^2,\ \omega_{\mathrm{p}} \in \mathbb{R}, \end{cases} \tag{51}$$

where the center G_{p} of rigid body B_h is known and $\mathbf{W}_{\mathbf{g}_{0h}} = \mathbf{W}_{\mathbf{g}_{0h}}^n$. A conjugate gradient algorithm for solving problem (51) is as follows:

Step 0: *Initialization*

$$\lambda^0 \in \Lambda_h \text{ is given;} \tag{52}$$

solve

$$\alpha \int_\Omega \mathbf{u}^0 \cdot \mathbf{v}\, \mathrm{dx} + \nu \int_\Omega \nabla\mathbf{u}^0 : \nabla\mathbf{v}\, \mathrm{dx} = \int_\Omega \mathbf{f}\cdot\mathbf{v}\, \mathrm{dx} + \langle \lambda^0, \mathbf{v} \rangle_{B_h}, \quad \forall \mathbf{v} \in \mathbf{W}_{0h};\ \mathbf{u}^0 \in \mathbf{W}_{\mathbf{g}_{0h}}, \tag{53}$$

$$\left(1 - \frac{\rho_{\mathrm{f}}}{\rho_{\mathrm{s}}}\right) M_{\mathrm{p}} \frac{V_{\mathrm{p}}^0 - V_{\mathrm{p}0}}{\Delta t} \cdot Y + \langle \lambda^0, Y \rangle_{B_h} = 0, \quad \forall Y \in \mathbb{R}^2;\ V_{\mathrm{p}}^0 \in \mathbb{R}^2, \tag{54}$$

$$\left(1-\frac{\rho_{\mathrm{f}}}{\rho_{\mathrm{s}}}\right)I_{\mathrm{p}}\frac{\omega_{\mathrm{p}}^{0}-\omega_{\mathrm{p}0}}{\Delta t}\,\theta+\left\langle\lambda^{0},\,\theta\times(\mathbf{x}-G_{\mathrm{p}})\right\rangle_{B_h}=0,\quad\forall\theta\in\mathbb{R};\ \omega_{\mathrm{p}}^{0}\in\mathbb{R},\tag{55}$$

then

$$\left\langle\mu,\,\mathbf{g}^{0}\right\rangle_{B_h}=\left\langle\mu,\,\mathbf{u}^{0}-V_{\mathrm{p}}^{0}-\omega_{\mathrm{p}}^{0}\times(\mathbf{x}-G_{\mathrm{p}})\right\rangle_{B_h},\quad\forall\mu\in\Lambda_h;\ \mathbf{g}^{0}\in\Lambda_h,\tag{56}$$

and set

$$\mathbf{w}^{0}=\mathbf{g}^{0}.\tag{57}$$

Then, for $m\geq 0$, assuming that λ^{m}, $\mathbf{u}^{m}$, V_{p}^{m}, ω_{p}^{m}, $\mathbf{w}^{m}$, $\mathbf{g}^{m}$ are known, we obtain λ^{m+1}, $\mathbf{u}^{m+1}$, V_{p}^{m+1}, $\omega_{\mathrm{p}}^{m+1}$, $\mathbf{w}^{m+1}$, $\mathbf{g}^{m+1}$ by

Step 1: *Descent*
Solve

$$\alpha\int_{\Omega}\bar{\mathbf{u}}^{m}\cdot\mathbf{v}\,\mathrm{d}\mathbf{x}+\nu\int_{\Omega}\nabla\bar{\mathbf{u}}^{m}:\nabla\mathbf{v}\,\mathrm{d}\mathbf{x}=\left\langle\mathbf{w}^{m},\,\mathbf{v}\right\rangle_{B_h},\quad\forall\mathbf{v}\in\mathbf{W}_{0h};\ \bar{\mathbf{u}}^{m}\in\mathbf{W}_{0h},\tag{58}$$

$$\left(1-\frac{\rho_{\mathrm{f}}}{\rho_{\mathrm{s}}}\right)\frac{M_{\mathrm{p}}}{\Delta t}\,\bar{V}_{\mathrm{p}}^{m}\cdot Y+\left\langle\mathbf{w}^{m},\,Y\right\rangle_{B_h}=0,\quad\forall Y\in\mathbb{R}^{2};\ \bar{V}_{\mathrm{p}}^{m}\in\mathbb{R}^{2},\tag{59}$$

$$\left(1-\frac{\rho_{\mathrm{f}}}{\rho_{\mathrm{s}}}\right)\frac{I_{\mathrm{p}}}{\Delta t}\,\bar{\omega}_{\mathrm{p}}^{m}\theta+\left\langle\mathbf{w}^{m},\,\theta\times(\mathbf{x}-G_{\mathrm{p}})\right\rangle_{B_h}=0,\quad\forall\theta\in\mathbb{R};\ \bar{\omega}_{\mathrm{p}}^{m}\in\mathbb{R},\tag{60}$$

and set

$$\left\langle\mu,\,\bar{\mathbf{g}}^{m}\right\rangle_{B_h}=\left\langle\mu,\,\bar{\mathbf{u}}^{m}-\bar{V}_{\mathrm{p}}^{m}-\bar{\omega}_{\mathrm{p}}^{m}\times(\mathbf{x}-G_{\mathrm{p}})\right\rangle_{B_h},\quad\forall\mu\in\Lambda_h;\ \bar{\mathbf{g}}^{m}\in\Lambda_h.\tag{61}$$

Then we compute

$$\rho_{m}=\left\langle\mathbf{g}^{m},\,\mathbf{g}^{m}\right\rangle_{B_h}/\left\langle\mathbf{w}^{m},\,\bar{\mathbf{g}}^{m}\right\rangle_{B_h},\tag{62}$$

and set

$$\lambda^{m+1}=\lambda^{m}-\rho_{m}\omega^{m},\tag{63}$$

$$\mathbf{u}^{m+1}=\mathbf{u}^{m}-\rho_{m}\bar{\mathbf{u}}^{m},\tag{64}$$

$$V_{\mathrm{p}}^{m+1}=V_{\mathrm{p}}^{m}-\rho_{m}\bar{V}_{\mathrm{p}}^{m},\tag{65}$$

$$\omega_{\mathrm{p}}^{m+1}=\omega_{\mathrm{p}}^{m}-\rho_{m}\bar{\omega}_{\mathrm{p}}^{m},\tag{66}$$

$$\mathbf{g}^{m+1}=\mathbf{g}^{m}-\rho_{m}\bar{\mathbf{g}}^{m}.\tag{67}$$

Step 2: *Testing the convergence and construction of the new descent direction*
If $\left\langle\mathbf{g}^{m+1},\,\mathbf{g}^{m+1}\right\rangle_{B_h}/\left\langle\mathbf{g}^{0},\,\mathbf{g}^{0}\right\rangle_{B_h}\leq\varepsilon$, then take $\mathbf{u}=\mathbf{u}^{m+1}$, $V_{\mathrm{p}}=V_{\mathrm{p}}^{m+1}$ and $\omega_{\mathrm{p}}=\omega_{\mathrm{p}}^{m+1}$. If not, compute

$$\gamma_{m}=\left\langle\mathbf{g}^{m+1},\,\mathbf{g}^{m+1}\right\rangle_{B_h}/\left\langle\mathbf{g}^{m},\,\mathbf{g}^{m+1}\right\rangle_{B_h},\tag{68}$$

and set

$$\mathbf{w}^{m+1}=\mathbf{g}^{m+1}+\gamma_{m}\mathbf{w}^{m}.\tag{69}$$

Do $m=m+1$ and go back to (58).

6. NUMERICAL EXPERIMENTS

6.1. Flow around an NACA0012 airfoil that has a fixed center of mass and is free to rotate due to hydrodynamical forces

Here we consider an incompressible viscous flow around an NACA0012 airfoil that has a fixed center of mass and is free to rotate due to hydrodynamical forces; the surrounding region Ω is the rectangle $(-4, 16) \times (-2, 2)$. The characteristic length, namely the airfoil length, is 1.009 and the fixed center of mass of the NACA0012 airfoil is at $(0.42, 0)$. Initial angular velocity and incident angle are zero. The density of the fluid is $\rho_f = 1.0$ and the density of the airfoil is $\rho_s = 1.1$. The viscosity of the fluid is $\nu_f = 0.01$. The initial condition for the fluid flow is $\mathbf{u}_0 = \mathbf{0}$ and the boundary data $\mathbf{g}_0$ is given by

$$\mathbf{g}_0(\mathbf{x}, t) = \begin{cases} \mathbf{0} & \text{if } x_2 = -2 \text{ or } 2, \\ (1 - e^{-50t}) \begin{pmatrix} 1 \\ 0 \end{pmatrix} & \text{if } x_1 = -4 \text{ or } 16, \end{cases}$$

for $t \geq 0$. Hence, the Reynolds number is about 101 with respect to the characteristic length of the NACA0012 airfoil and the maximal inflow speed. In this case we have chosen two sets of time step and mesh size to validate the simulation results. In the first set, the time step is $\Delta t = 0.0015$ and the mesh size for the velocity field is $h_v = 1/64$ (there are 329217 nodes). In the second set, the time step is $\Delta t = 0.001$ and the mesh size for the velocity field is $h_v = 1/96$ (there are 739585 nodes). The mesh size for pressure is always $h_p = 2h_v$.

To enforce the rigid body motion inside the airfoil at each time step, using the discrete multiplier space defined in (32), we have taken all the grid points from the velocity grid contained in the NACA0012 at that time completed by a selected set of points belonging to the boundary of the airfoil (see Figure 2) and then used a scalar product over $\Lambda_h(t)$, such as the one defined by (33).

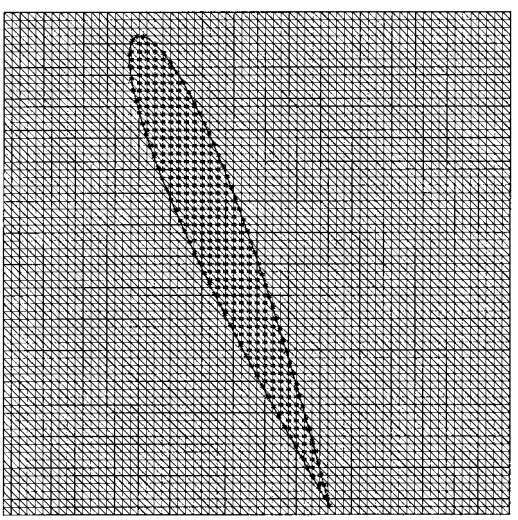

Figure 2. Part of the velocity mesh and example of mesh points used in (32) for enforcing the rigid body motion in the NACA0012 airfoil.

The NACA0012 airfoil is fixed up to $t = 1$. A steady flow around it is obtained. After $t = 1$, we allow the NACA0012 airfoil to rotate freely. In Figure 3, we observe that the histories corresponding to the two sets of time step and mesh size are in very good agreement. The NACA0012 airfoil intends to keep its broadside perpendicular to the inflow direction, which is a stable position for non-circular particles settling in a channel at small Reynolds number [28].

In the second test case, we have used the same data and parameters with the exception of the viscosity; we have taken $\nu_f = 0.00125$ (the Reynolds number is now about 807). The time step is $\Delta t = 0.001$ and the mesh size for the velocity is $h_v = 1/96$ which is required to catch the velocity field close to the leading edge of the NACA0012 airfoil without losing stability (when we used $h_v = 1/64$, the numerical solution blows up near the leading edge of the airfoil). In the simulation, the number of iterations for the divergence-free projection problem (42) is 16, the number of iterations for the linearized advection–diffusion problem (43) is two, and the one for the rigid body motion projection varies from 65 to 238. The first two numbers of iterations are almost independent of the mesh size; the last one is quite large and we are working to reduce it via the use of a H^1-scalar product, such as the ones defined in remark 2.2. The histories of the angle and angular velocity of the NACA0012 airfoil are shown in Figure 4. The NACA0012 airfoil is completely fixed without possible rotation up to $t = 2$ (see Figure 5). After $t = 2$ we allow the NACA0012 airfoil to rotate freely. The flow fields and the vorticity density at times $t = 7$, 9, 11, 13, are shown in Plates 1 and 2. We observe then that the NACA0012 airfoil oscillates from about $-70°$ to 74°.

In the case of a Reynolds number of 101, a code of size 41 Mb takes about 53 s at each time step on one node of an IBM SP2 for the coarse mesh ($h_v = 1/64$ and $\Delta t = 0.0015$). For the fine mesh ($h_v = 1/96$ and $\Delta t = 0.001$), a code of size 93 Mb takes about 107 s at each time step on one node of an IBM SP2.

Remark 6.1

For the test case discussed here, the fact that we used a uniform fine mesh may appear as a drawback. Actually this test problem was considered for validation purpose and also to show

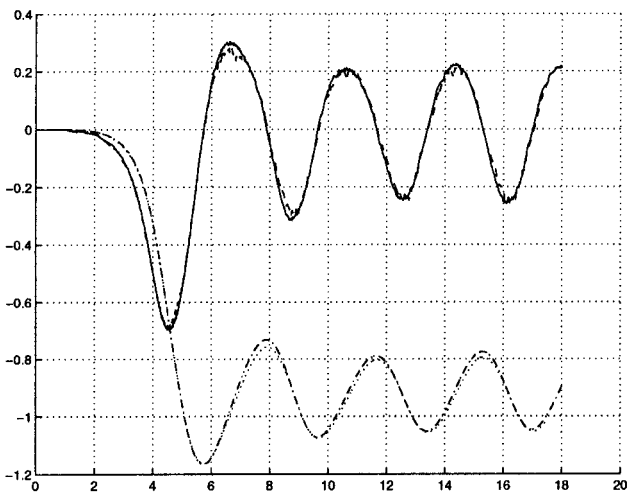

Figure 3. Histories of the angle (dashed–dotted line for $h_v = 1/96$ and dotted line for $h_v = 1/64$) and angular velocity (solid line for $h_v = 1/96$ and dashed line for $h_v = 1/64$) of the NACA0012 airfoil at $Re = 101$.

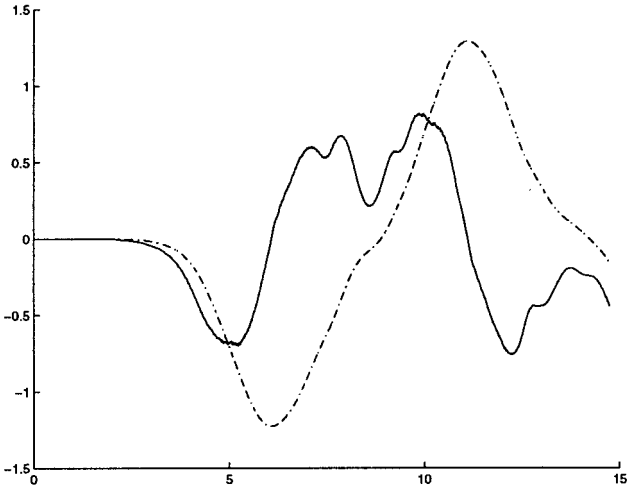

Figure 4. Histories of the angle (dashed–dotted line) and angular velocity (solid line) of the NACA0012 airfoil at $Re = 807$.

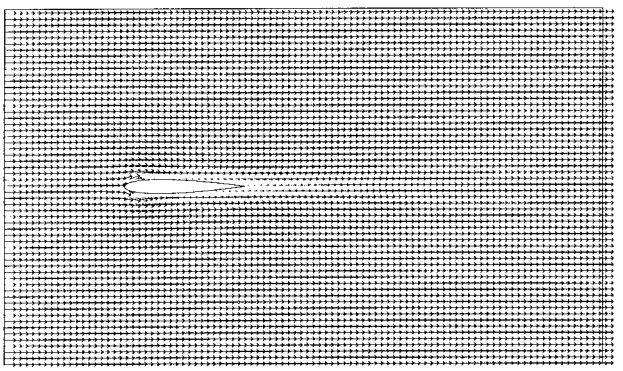

Figure 5. Flow field around the NACA0012 airfoil at $t = 2$.

that our methodology can handle non-circular bodies. Also when simulating the flow of mixtures with over 100 particles highly dispersed in the flow region (see Figures 10 and 11), which is the main goal of the distributed Lagrange multiplier method discussed here, using a fine uniform mesh everywhere is not a drawback anymore (particularly for a flow where the ratio of solid volume/fluid volume is of the order of one, or more).

Remark 6.2

For the above test problem, we have imposed $\mathbf{u} = \mathbf{0}$ on the top and bottom boundaries of Ω. Actually, with the methodology discussed in this article, there would have been no problem imposing $\mathbf{u} = \mathbf{u}_\infty$ ($\neq \mathbf{0}$) on the inflow, top and bottom boundaries of Ω, and $\nu_f(\partial \mathbf{u}/\partial \mathbf{n}) - \mathbf{n}p = \mathbf{0}$ (or $\sigma \mathbf{n} = \mathbf{0}$) on the outflow boundary. We can justify the boundary conditions used here by the fact that experimental results concerning the flow around cylinders are obtained by putting the cylinders in channels where they are fixed or free to rotate, the boundary conditions on the boundary of the channels being close to those used in the article.

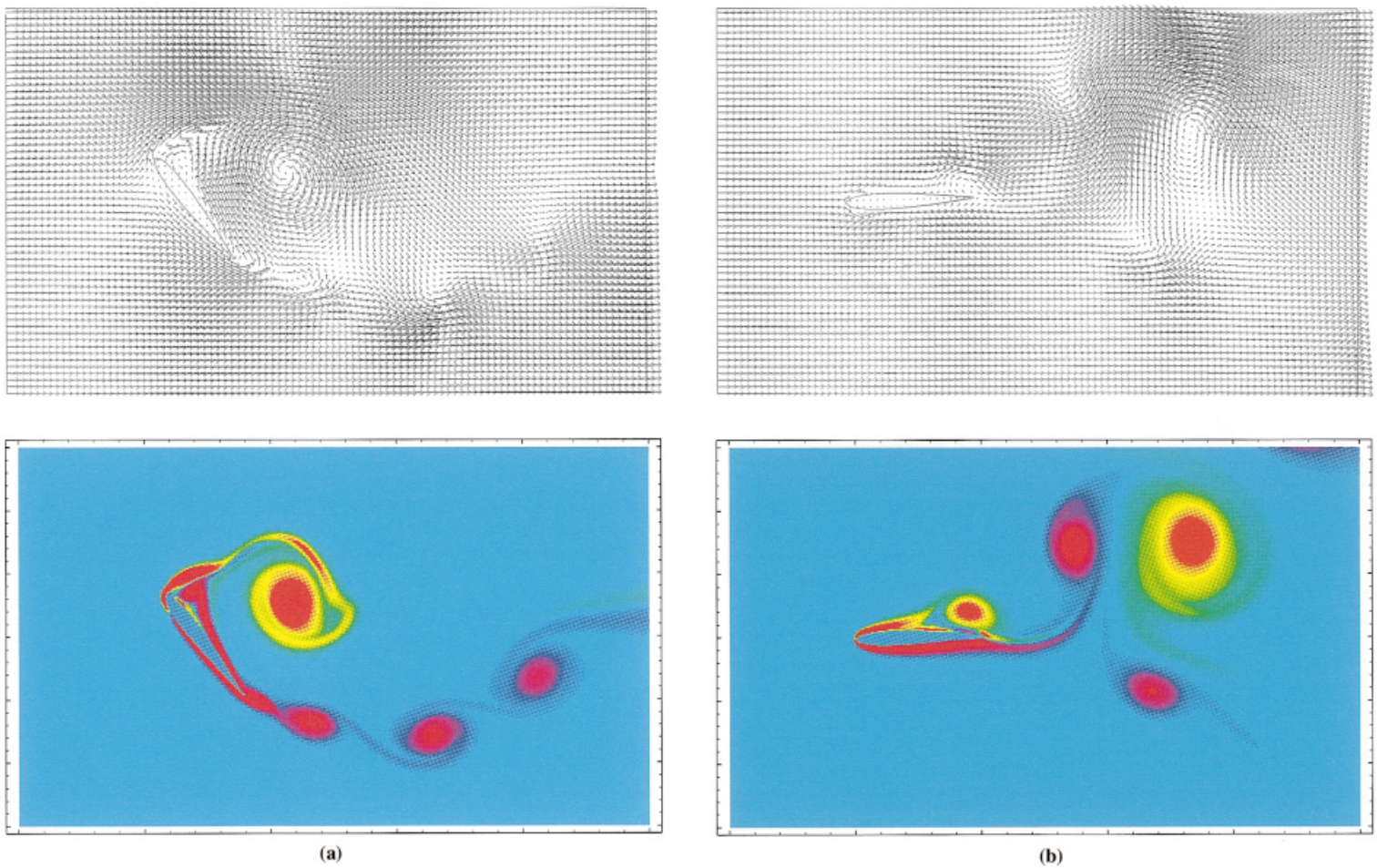

Plate 1. Flow field visualization (above) and density plot of the vorticity (below) around the NACA0012 airfoil at (a) $t = 7$, (b) $t = 9$.

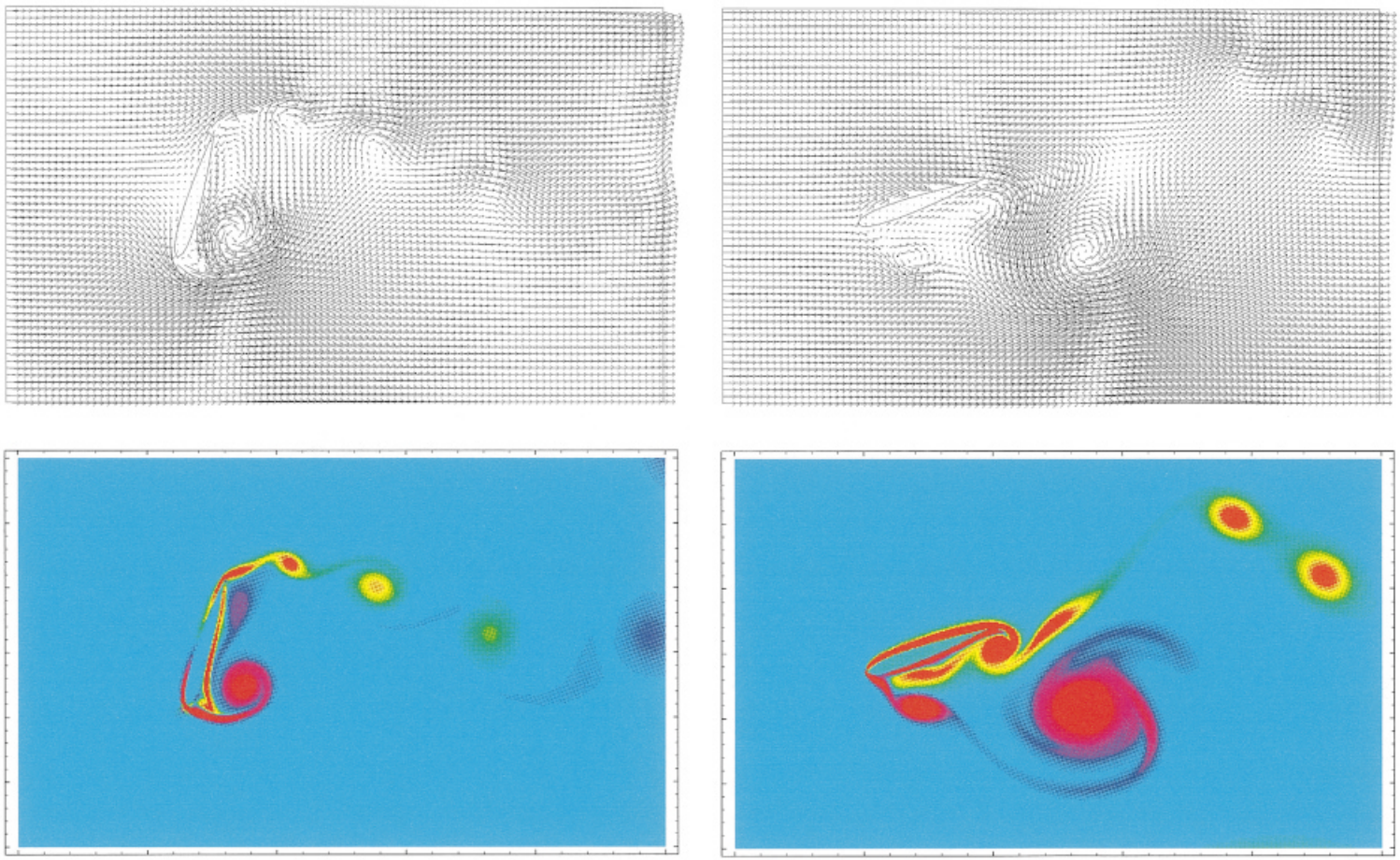

Plate 2. Flow field visualization (above) and density plot of the vorticity (below) around the NACA0012 airfoil at (a) $t = 11$, (b) $t = 13$.

Remark 6.3
Using the parallelization techniques developed by Sameh and Sarin, the computational times given above have been divided by factors of the order of 10; see [29] for details.

6.2. A 200 particles case

The second test problem that we consider concerns the simulation of the motion of 200 sedimenting cylinders in the closed channel $\Omega = (0, 6) \times (0, 6)$. The diameter d of the cylinders is 0.125 and the position of the cylinders at time $t = 0$ is shown in Figure 6. The solid fraction in this test case is 27.27%. Initial velocity and angular velocity of the cylinders are $V^0_{p,i} = \mathbf{0}$, $\omega^0_{p,i} = 0$ for $i = 1, \ldots, 200$. The density of the fluid is $\rho_f = 1.0$ and the density of the cylinders is $\rho_s = 1.01$. The viscosity of the fluid is $\nu_f = 0.01$. The initial condition for the fluid flow is $\mathbf{u}_0 = \mathbf{0}$ and $\mathbf{g}_0(t) = \mathbf{0}$, $\forall t \geq 0$. In this test case, we also have chosen two sets of time step and mesh size to validate the simulation results. In the first set, the time step is $\Delta t = 0.0015$ and the mesh size for the velocity field is $h_v = 1/80$ (there are 231 361 nodes). In the second set, the time step is $\Delta t = 0.001$ and the mesh size for the velocity field is $h_v = 1/120$ (there are 519 841 nodes). The mesh size for pressure is always $h_p = 2h_v$.

The histories of the averaged vertical and horizontal translational cylinder velocities for these two sets of time step and mesh size are shown in Figure 7. The histories of the averaged

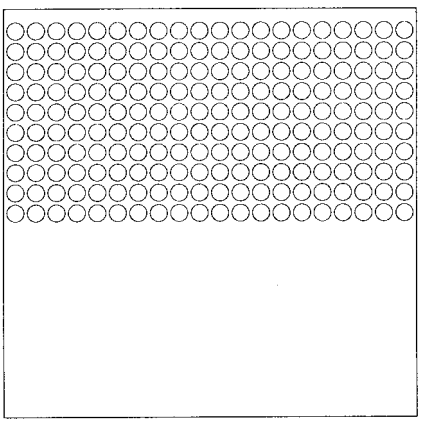

Figure 6. Sedimentation of 200 circular particles: initial position of the cylinders.

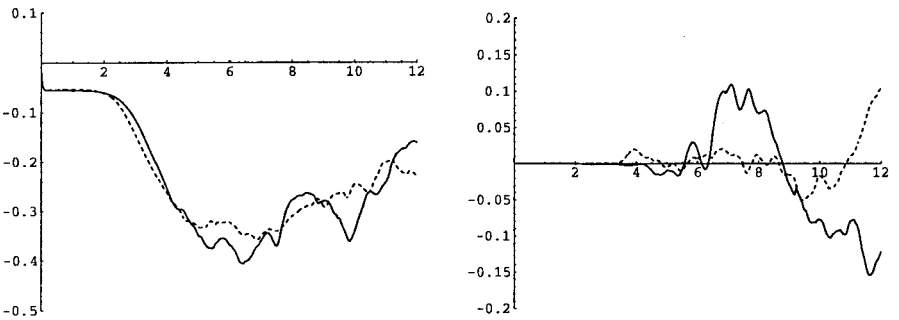

Figure 7. Histories of the averaged vertical (left) and horizontal (right) translational velocities of the cylinders obtained using ($h_v = 1/80$, $\Delta t = 0.0015$) (dashed lines) and ($h_v = 1/120$, $\Delta t = 0.001$) (solid lines).

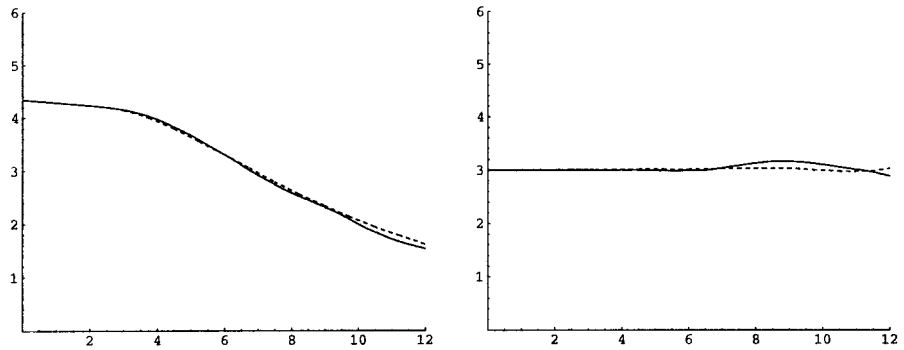

Figure 8. Histories of the averaged y co-ordinates (left) and x co-ordinates (right) of the cylinders obtained using ($h_v = 1/80$, $\Delta t = 0.0015$) (dashed lines) and ($h_v = 1/120$, $\Delta t = 0.001$) (solid lines).

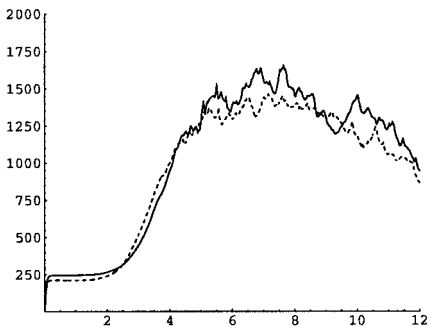

Figure 9. Histories of the flow kinetic energy obtained using ($h_v = 1/80$, $\Delta t = 0.0015$) (dashed lines) and ($h_v = 1/120$, $\Delta t = 0.001$) (solid lines).

y co-ordinates and x co-ordinates of the cylinders are shown in Figure 8. The histories of the computed flow kinetic energy are shown in Figure 9. We find a good correlation between these results obtained from the two sets of time step and mesh size until the symmetry breakings occur (see Figure 10) between $t = 4$ and $t = 5$.

In this case, a code of size 40 Mb takes about 47 s at each time step on a DEC personal workstation 500au for the coarse mesh ($h_v = 1/80$ and $\Delta t = 0.0015$). For the fine mesh ($h_v = 1/120$ and $\Delta t = 0.001$), a code of size 81 Mb takes about 99 s at each time step on the same DEC workstation. Remark 6.3 still holds.

Remark 6.4

We observe that if the mesh size and the time step are modified by a factor of 1.5 there is no drastic change in the solutions concerning the settling of the cylinders, at least for the average quantities shown in Figures 7–9. One has to realize that many bifurcation phenomena are taking place when particles get close (kissing) and then separate (tumbling); the individual behavior seems to be of the chaotic type, not surprising after all for a 200-body problem.

6.3. A 1008 particles case

The third test problem that we consider concerns the simulation of the motion of 1008 sedimenting cylinders in the closed channel $\Omega = (0, 2) \times (0, 4)$. The diameter d of the cylinders

is 0.0625 and the position of the cylinders at time $t = 0$ is shown in Figure 11. The solid fraction in this test case is 38.66%. Initial velocity and angular velocity of the cylinders are $V_{\mathrm{p},i}^0 = \mathbf{0}$, $\omega_{\mathrm{p},i}^0 = 0$ for $i = 1, \ldots, 1008$. The density of the fluid is $\rho_{\mathrm{f}} = 1.0$ and the density of the cylinders is $\rho_{\mathrm{s}} = 1.01$. The viscosity of the fluid is $\nu_{\mathrm{f}} = 0.01$. The initial condition for the fluid flow is $\mathbf{u}_0 = \mathbf{0}$ and $\mathbf{g}_0(t) = \mathbf{0}$, $\forall t \geq 0$. The time step is $\Delta t = 0.001$. The mesh size for the velocity field is $h_{\mathrm{v}} = 1/256$ (there are 525835 nodes). The mesh size for pressure is $h_{\mathrm{p}} = 1/128$ (131841 nodes). In this test case, where many particles move around, a fine mesh is required essentially everywhere. We have chosen $\alpha = 1$ and $\beta = 0$ in the Marchuk–Yanenko scheme. The number of iterations for the divergence-free projection problem varies from 12 to 14, the number of iterations for the linearized advection–diffusion problem is five, and the one for the rigid body motion projection is about seven. Those numbers of iterations are almost independent of the mesh size and of the number of particles. The evolution of the 1008 cylinders

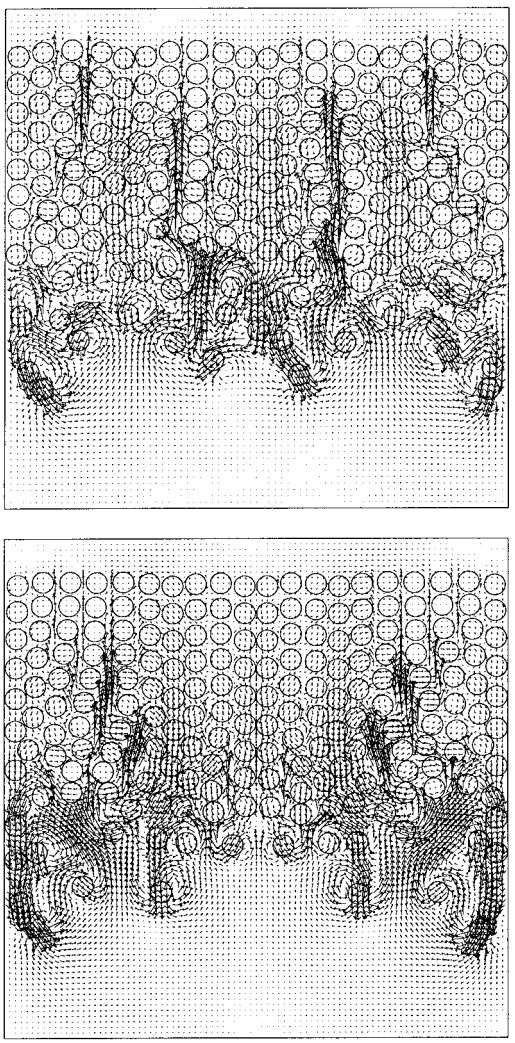

Figure 10. Sedimentation of 200 circular particles: $t = 4$, obtained using ($h_{\mathrm{v}} = 1/80$, $\Delta t = 0.0015$) (top) and ($h_{\mathrm{v}} = 1/120$, $\Delta t = 0.001$) (bottom).

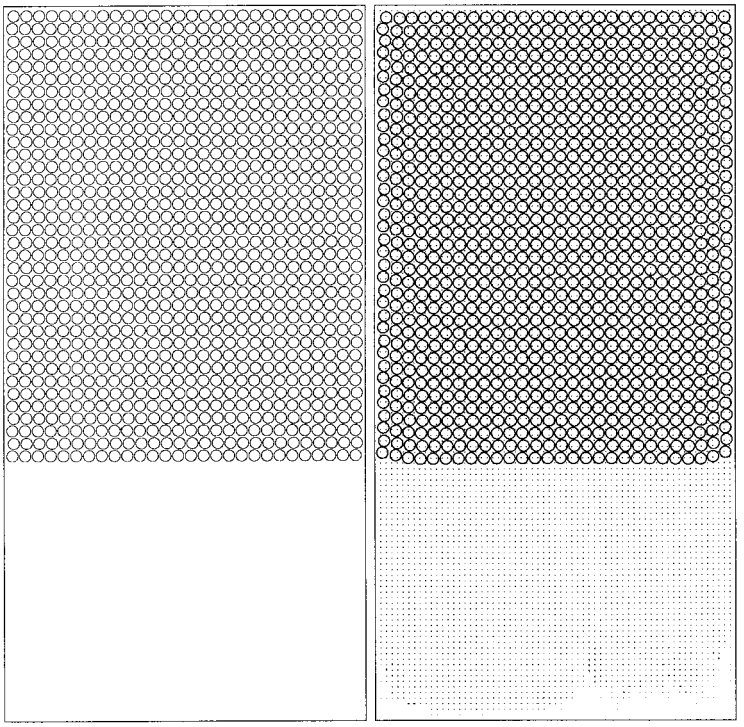

Figure 11. Sedimentation of 1008 circular particles: $t = 0$, 1 (left to right).

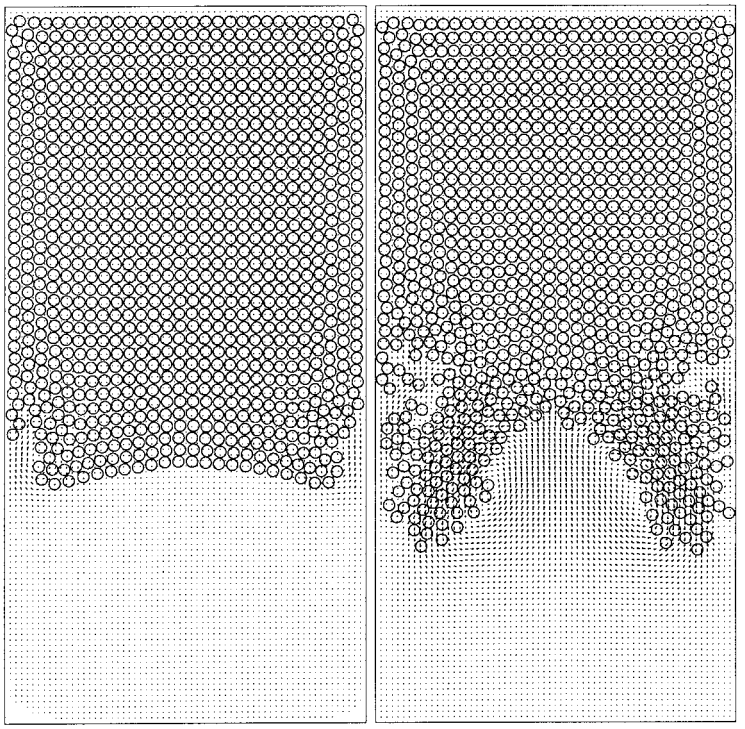

Figure 12. Sedimentation of 1008 circular particles: $t = 2$, 3 (left to right).

sedimenting in the closed channel is shown in Figures 11–15. The maximal particle Reynolds number in the entire evolution is 17.44. The slightly wavy shape of the interface observed at $t = 1$ in Figure 11, is typical of the onset of a Rayleigh–Taylor instability. When t is between 1 and 2, two small eddies are forming close to the left wall and the right wall and some particles are pulling down fast by these two eddies. Then other two stronger eddies are forming at the lower center of the channel for t between 2 and 4; they push some particles almost to the top wall of the channel. The above figures clearly show a fingering phenomenon, followed by a symmetry breaking. At the end all particles are settled at the bottom of the channel.

6.4. A three-dimensional case with two identical spherical particles

The fourth test problem considered here concerns the simulation of the motion of two sedimenting balls in a rectangular cylinder. A two-dimensional analog of this test case problem has been (successfully) investigated in [30] using similar techniques. The initial computational domain is $\Omega = (0, 1) \times (0, 1) \times (-1, 1.5)$, then it moves with the center of the lower ball. The diameter d of the two balls is $1/6$ and the position of the balls at time $t = 0$ is shown in Figure 16. The initial velocity and angular velocity of the balls are zero. The density of the fluid is $\rho_f = 1.0$ and the density of the balls is $\rho_s = 1.04$. The viscosity of the fluid is $\nu_f = 0.01$. The initial condition for the fluid flow is $\mathbf{u}_0 = \mathbf{0}$ The mesh size for the velocity field is $h_v = 1/60$ (561 871 nodes). The mesh size for pressure is $h_p = 1/30$ (73 036 nodes). The time step is $\Delta t = 0.001$. The simulation takes about 80 s per time step on a DEC personal workstation 500au. The maximal particle Reynolds number in the entire evolution is 47.57. In Figures 16–18 (we have followed these two balls to draw those figure), we can see the fundamental

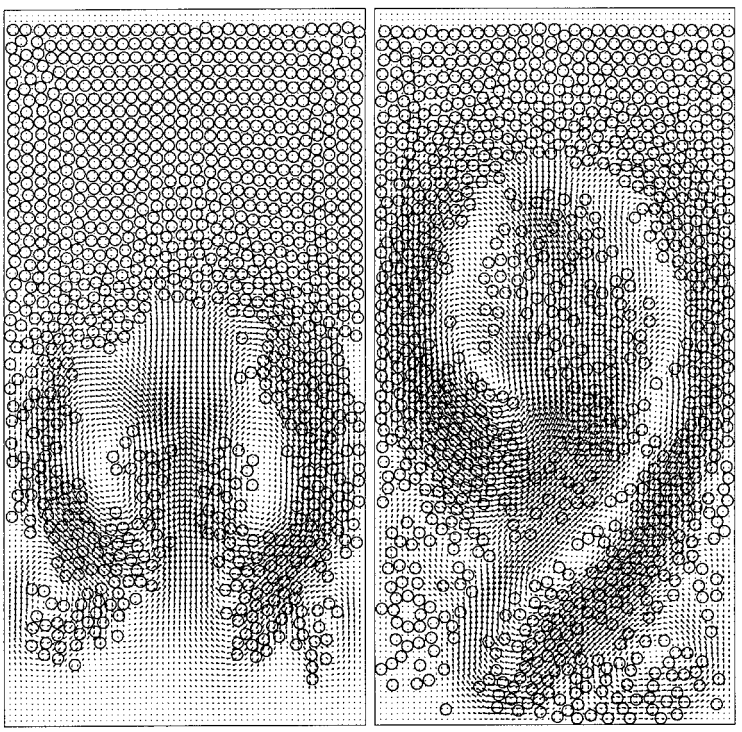

Figure 13. Sedimentation of 1008 circular particles: $t = 4$, 5 (left to right).

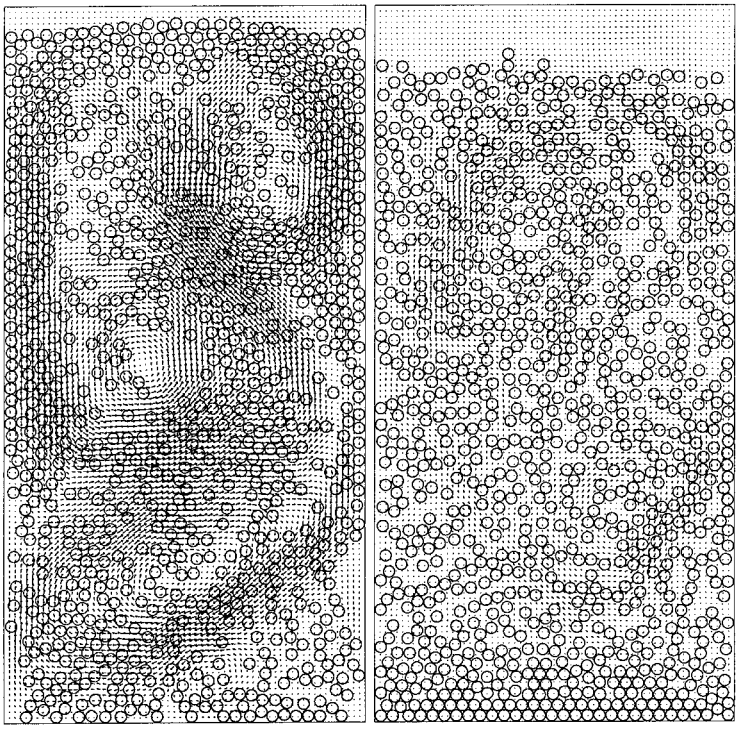

Figure 14. Sedimentation of 1008 circular particles: $t = 6$, 10 (left to right).

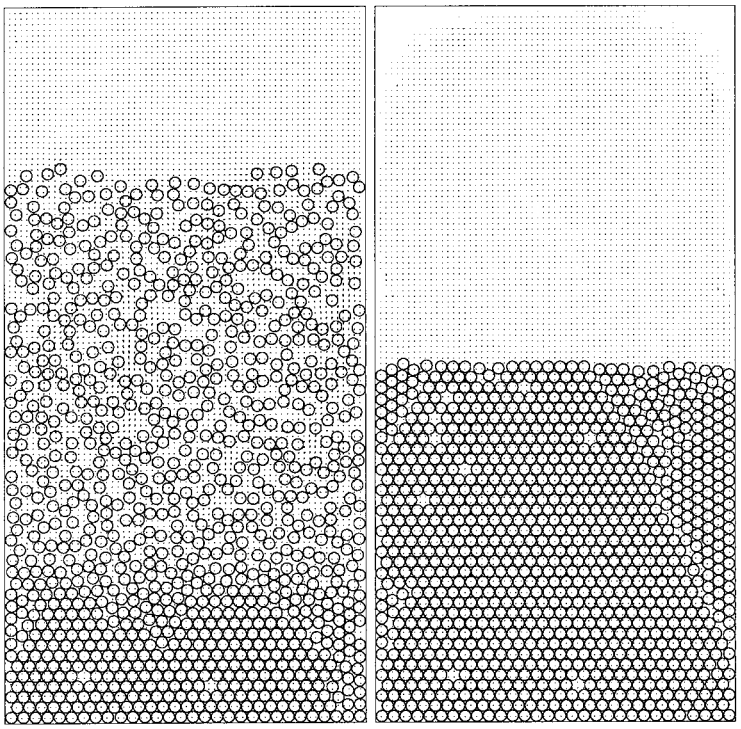

Figure 15. Sedimentation of 1008 circular particles: $t = 20$, 48 (left to right).

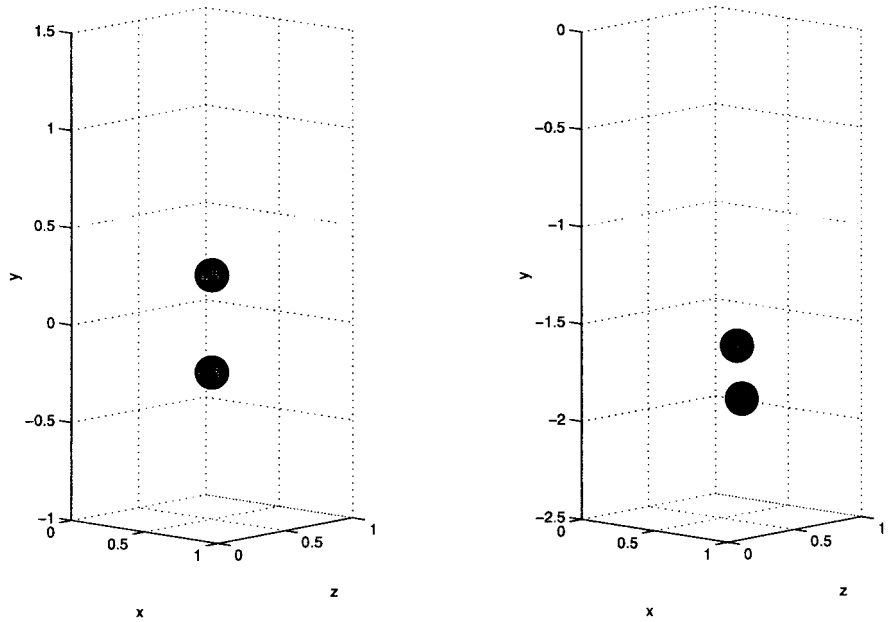

Figure 16. Particle position at $t = 0$, 1 (left to right).

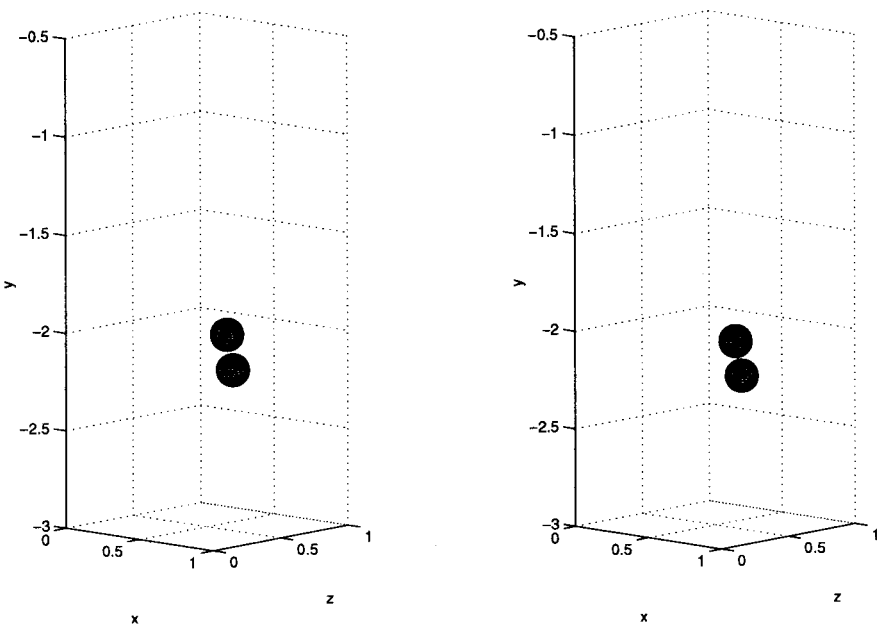

Figure 17. Particle position at $t = 1.149$, 1.169 (left to right).

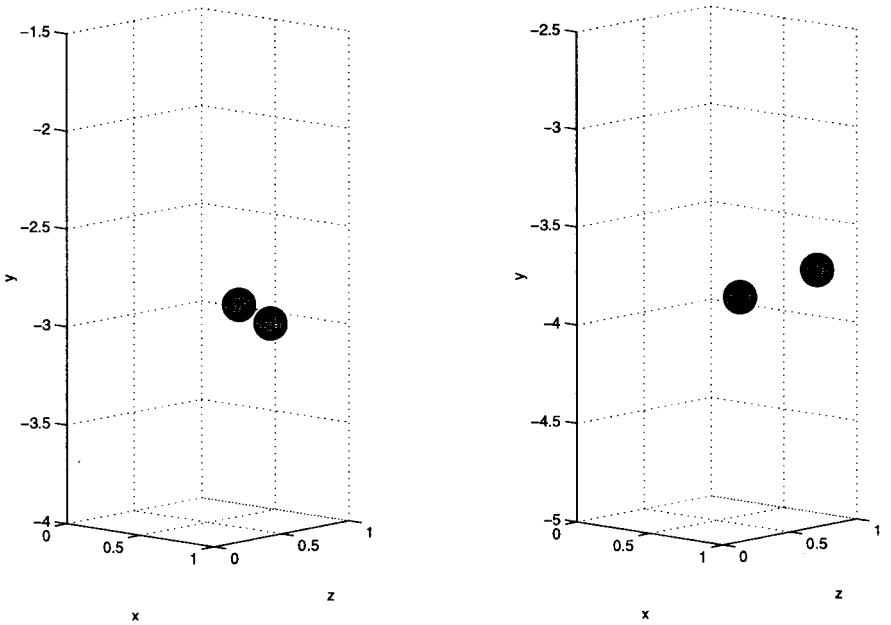

Figure 18. Particle position at $t = 1.5$, 2 (left to right).

features of the two (initially close) sedimenting balls, i.e. drafting, kissing and tumbling [31]. We observe that a symmetry breaking occurs before the kissing; with a smaller *Re*, this symmetry breaking would occur after the kissing. Using smaller h and Δt brings essentially the same results.

7. CONCLUSION

We have presented in this article a distributed Lagrange multiplier-based fictitious domain method for the simulation of flow with moving boundaries. Compared with the one [32] discussed earlier it allows the simulation of fairly complicated flow phenomena, such as particulate flow, including sedimentation. Actually, some preliminary experiments have shown the potential of this method for the direct simulation of fluidization, which is in some sense the inverse phenomenon of sedimentation; the results already obtained look promising. Other goals include: three-dimensional particulate flow with a large number of particles of different sizes and shapes, particulate flow for viscoelastic liquids such as Oldroyd B, etc.

ACKNOWLEDGMENTS

The authors acknowledge the helpful comments and suggestions of E.J. Dean, V. Girault, J. He, Y. Kuznetsov, B. Maury and G. Rodin and also the support of NEC concerning the use of an SX-3 supercomputer. They acknowledge the support of the NSF under HPCC Grand Challenge Grant ECS-9527123, NSF (Grants DMS 8822522, DMS 9112847, DMS 9217374), DRET (Grant 89424), DARPA (Contracts AFOSR F49620-89-C0125, AFOSR-90-0334), the

Texas Board of Higher Education (Grants 003652156ARP and 003652146ATP) and the University of Houston (PEER grant 1-27682). The most helpful comments and suggestions of the two referees are also acknowledged.

REFERENCES

1. R. Glowinski, T.-W. Pan and J. Périaux, 'A fictitious domain method for Dirichlet problem and applications', *Comput. Methods Appl. Mech. Eng.*, **111**, 283–303 (1994).
2. R. Glowinski, T.-W. Pan and J. Périaux, 'A fictitious domain method for external incompressible viscous flow modeled by Navier–Stokes equations', *Comput. Methods Appl. Mech. Eng.*, **112**, 133–148 (1994).
3. R. Glowinski, T.-W. Pan and J. Périaux, 'A Lagrange multiplier/fictitious domain method for the Dirichlet problem. Generalization to some flow problems', *Jpn. J. Ind. Appl. Math.*, **12**, 87–108 (1995).
4. R. Glowinski, T.-W. Pan and J. Périaux, 'Fictitious domain methods for incompressible viscous flow around moving rigid bodies', in J.R. Whiteman (ed.), *The Mathematics of Finite Elements and Applications*, *Highlight 1996*, Wiley, Chichester, 1997, pp. 155–174.
5. R. Glowinski, T.-W. Pan and J. Périaux, 'A Lagrange multiplier/fictitious domain method for the numerical simulation of incompressible viscous flow around moving rigid bodies (I): The case where the rigid body motions are known *a priori*', *C. R. Acad. Sci. Paris*, **324**, 361–369 (1997).
6. R. Glowinski, T.-W. Pan and J. Périaux, 'Distributed Lagrange multiplier methods for incompressible viscous flow around moving rigid bodies', *Comput. Methods Appl. Mech. Eng.*, **151**, 181–194 (1998).
7. A. Johnson and T. Tezduyar, '3D Simulation of fluid–rigid body interactions with the number of rigid bodies reaching 100', *Comput. Methods Appl. Mech. Eng.*, **145**, 301–321 (1997).
8. H.H. Hu, 'Direct simulation of flows of solid–liquid mixtures', *Int. J. Multiphase Flow*, **22**, 335–352 (1996).
9. C.S. Peskin, 'Numerical analysis of blood flow in the heart', *J. Comput. Phys.*, **25**, 220–252 (1977).
10. C.S. Peskin and D.M. McQueen, 'Modeling prosthetic heart valves for numerical analysis of blood flow in the heart', *J. Comput. Phys.*, **37**, 113–132 (1980).
11. C.S. Peskin, 'Lectures on mathematical aspects of physiology', *Lectures Appl. Math.*, **19**, 69–107 (1981).
12. R.J. LeVeque and Z. Li, 'The immersed interface method for elliptic equations with discontinuous coefficients and singular sources', *SIAM J. Numer. Anal.*, **31**, 1019–1044 (1994).
13. R.J. LeVeque and Z. Li, 'Immersed interface methods for Stokes flow with elastic boundaries or surface tension', *SIAM J. Sci. Comput.*, **18**, 709–735 (1997).
14. R. Glowinski, T.-W. Pan, T. Hesla, D.D. Joseph and J. Périaux, 'A fictitious domain method with distributed Lagrange multipliers for the numerical simulation of particulate flows', in J. Mandel, C. Faraht and X.-C. Cai (eds.), *Domain Decomposition Methods 10*, AMS, Providence, RI, 1998, pp. 121–137.
15. B.A. Maury, 'A many-body lubrication model', *C. R. Acad. Sci. Paris*, **325**, 1053–1058 (1997).
16. T.I. Hesla, 'The dynamical simulation of two-dimensional fluid/rigid body systems', Unpublished notes, 1991.
17. F. Bertrand, P.A. Tanguy and F. Thibault, 'A three-dimensional fictitious domain method for incompressible fluid flow problem', *Int. J. Numer. Methods Fluids*, **25**, 719–736 (1997).
18. F. Brezzi and M. Fortin, *Mixed and Hybrid Finite Element Methods*, Springer, New York, 1991.
19. J.E. Roberts and J.M. Thomas, 'Mixed and hybrid methods', in P.G. Ciarlet and J.L. Lions (eds.), *Handbook of Numerical Analysis*, Vol. II, North-Holland, Amsterdam, 1991, pp. 523–639.
20. A.J. Chorin, 'A numerical method for solving incompressible viscous flow problems', *J. Comput. Phys.*, **2**, 12–26 (1967).
21. A.J. Chorin, 'On the convergence and approximation of discrete approximation to the Navier–Stokes equations', *Math. Comput.*, **23**, 341–353 (1968).
22. A.J. Chorin, 'Numerical study of slightly viscous flow', *J. Fluid Mech.*, **57**, 785–796 (1973).
23. R. Glowinski and O. Pironneau, 'Finite element methods for Navier–Stokes equations', *Annu. Rev. Fluid Mech.*, **24**, 167–204 (1992).
24. S. Turek, 'A comparative study of time-stepping techniques for the incompressible Navier–Stokes equations: from fully implicit non-linear schemes to semi-implicit projection methods', *Int. J. Numer. Math. Fluids*, **22**, 987–1011 (1996).
25. P.M. Gresho and R.L. Sani, *Incompressible Flow and the Finite Element Method*, Wiley, Chichester, 1998.
26. G.I. Marchuk, 'Splitting and alternate direction methods', in P.G. Ciarlet and J.L. Lions (eds.), *Handbook of Numerical Analysis*, Vol. I, North-Holland, Amsterdam, 1990, pp. 197–462.
27. R. Glowinski, *Numerical Methods for Non-linear Variational Problems*, Springer, New York, 1984.
28. H. Hu, D.D. Joseph and A.F. Fortes, 'Experiments and direct simulation of fluid particle motions', *Int. Vid. J. Eng. Res.*, **2**, 17 (1992).
29. T.W. Pan, V. Sarin, R. Glowinski, A. Sameh and J. Periaux, 'A fictitious domain method with distributed Lagrange multipliers for the numerical simulation of particular flow and its parallel implementation', *Proceedings of Parallel CFD '98* (to appear).

30. R. Glowinski, T.I. Hesla, D. D. Joseph, T.W. Pan and J. Périaux, 'Distributed Lagrange multiplier methods for particulate flows', in M.O. Bristeau, G. Etgen, W. Fitzgibbon, J.L. Lions, J. Périaux and M.F. Wheeler (eds.), *Computational Science for the 21st Century*, Wiley, Chichester, 1997, pp. 270–279.
31. A.F. Fortes, D.D. Joseph and T.S. Lundgren, 'Non-linear mechanics of fluidization of beds of spherical particles', *J. Fluid Mech.*, **177**, 467–483 (1987).
32. R. Glowinski, A. J. Kearsley, T.-W. Pan and J. Périaux, 'Numerical simulation and optimal shape for viscous flow by fictitious domain method', *Int. J. Numer. Methods Fluids*, **20**, 695–711 (1995).

